ROLES OF MACROPHAGES IN MECHANICAL LOAD-INDUCED BONE FORMATION ON 3D SILK FIBROIN SCAFFOLDS

Master Thesis

submitted for the degree of
Master of Science in Nanosciences
at the University of Basel

Melanie Burkhardt

Advisor
Dr. Ming Chang

Supervisors
University of Basel: Prof. Dr. Ueli Aebi
ETH Zürich: Prof. Dr. Ralph Müller

Institute for Biomechanics, D-MAVT
ETH Zürich

2010

Eidgenössische Technische Hochschule Zürich
Swiss Federal Institute of Technology Zurich

ETH Zurich
Institute for Biomechanics
Wolfgang-Pauli-Strasse 10
8093 Zürich, Switzerland

MASTERS THESIS
Nanosciences, University of Basel, HS/FS 2009/2010
Melanie Burkhardt

ROLES OF MACROPHAGES IN MECHANICAL LOAD-INDUCED BONE FORMATION ON 3D SILK FIBROIN SCAFFOLDS

1. INTRODUCTION

Mechanical loading is one of the most important physiological/environmental factors that governs the final mass and architecture of bone. However, definitive identification of the mechanosensitive cells and the cellular and molecular pathways by which applied mechanical load is transduced into anabolic signals, remain to be determined. The emerging new field of osteoimmunology describes the complex regulatory interactions between bone cells and cells of the immune system. Macrophages are heterogeneous mononuclear phagocytes that play important roles in innate and adaptive immunity as well as contribute to ongoing physiological processes and tissue repair. Macrophages had been characterized in the bone microenvironment and shown to promote osteoblast bone formation *in vitro*. The hypothesis of this project is that macrophages play a role in sensing mechanical strain and transducing the subsequent anabolic signals. Specifically, a model of *in vitro* mechanical stimulation induced bone formation will be established using an osteoblast cell line on 3D silk fibroin scaffolds in bioreactors. The possible ability of macrophages to facilitate osteoblast bone formation in response to mechanical strain will be investigated. Changes in bone formation will be monitored using micro-computed tomography (microCT) and cellular phenotypes will be determined using immunohistochemistry and histology.

2. TASK LIST

1. Literature research on bone adaptation to mechanical loading
2. Introduction into the relevant methodologies
3. Definition of a time schedule of the study
4. Selection and validation of the most promising methods/culture conditions
5. Production of silk fibroin scaffolds
6. Cell culture
7. Mechanical stimulation of cell culture
8. MicroCT analysis of cell culture
9. Data evaluation and analysis
10. Detailed project report and project presentation

3. LITERATURE

1 Duncan et al., *Calc Tiss Int* **57** (5), 344 (1995)
2 Biewener, et al., *Bone* **19** (1), 1 (1996).
3 Arron et al., *Nature* **408** (6812), 535 (2000).

4 Chang, et al., *J Immunol* **181** (2), 1232 (2008).
5 Freyria, et al., *Tiss Eng* **11** (5-6), 674 (2005).
6 Hagenmüller, et al., *Tiss Eng* **14**, 761 (2008).

Master Thesis, HS/FS 2009/2010

Start of thesis:	01.09.2009
End of thesis:	31.03.2010

Thesis Supervisor:

(Signature): _____ Place, Date:

Prof. Ralph Müller
Institute for Biomechanics, D-MAVT

Thesis Advisor(s):

(Signature): _____ Place, Date:

Dr. Ming Chang
Institute for Biomechanics, D-MAVT

Acknowledgments

First of all I would like to thank my advisor Dr. Ming Chang for her help and friendship during my work. You always helped me if I had any questions or problems and I really could learn a lot from you. Special thanks goes also to the other members of the skeletal tissue engineering group, as you all have been there to answer my specific questions. To mention is Benjamin Thimm, who especially helped me doing SEM measurements, Elena Schuh, who helped me whenever I needed some advice, Silke Wüest, who showed me how to produce silk fibroin scaffolds and not to forget Dr. Sandra Hofmann who had always an answer to my questions.

Then I would like to thank Prof. Ralph Müller, who made it possible, that I could do my master thesis at the Institute for Biomechanics here at the ETH Zürich. And thanks go to Prof. Ueli Aebi from the University of Basel who supported me from my home University in Basel.

I then would like to thank all the people who encouraged me during my thesis, my family, my friends and also the other students at the Institute, who were all there for me whenever I needed them.

Abstract

Tissue engineering is one approach, which aims to provide grafts for regenerative medicine, as there is an increasing need of grafts. The new approach would take cells from the patient, differentiate and grow them in vitro into the needed tissue graft and implant it back into the patient helping to reduce risks of viral contamination and immune reaction. Therefore, in a tissue engineered approach bone tissue formation of MC3T3 osteoblasts on 3D silk fibroin (SF) scaffolds was optimized with using mechanical load-induced stimulation and co-culturing of RAW 264.7 macrophages. Silk fibroin from *B. mori*, which is shown to be biocompatible, biodegradable and has suitable mechanical properties for bone formation was used to produce porous SF scaffolds. Scaffolds were produced with a salt-leaching method using porogens of 112-224 μm or 224-315 μm in diameter to get small or large pore size SF scaffolds. Topography and morphology of the two scaffold types produced from three different SF batches were analyzed by scanning electron microcopy and micro-computed tomography (microCT). MC3T3 osteoblast cell line was cultured in 24-well plates to investigate the best of three different cell seeding densities (1.2, 2.4 or 5.2 x 10^4 cells/well) and two osteogenic media (BGJb or MEM α with AA and β-G). Analysis of cell proliferation, cell differentiation, as well as collagen production and mineralization have been quantified, indicating that the lowest seeding density is sufficient and that BGJb with AA and β-G is the best osteogenic media for MC3T3 osteoblasts. MC3T3 were cultured on small and large pore size SF scaffolds in static bioreactors in osteogenic BGJb media for 33 days. Mineralization was monitored with microCT, DNA content, collagen production and mineralization were quantified with assays at the end of culture. Cell-scaffold constructs were analyzed with either SEM or embedded in paraffin for histology. Increasing mineralization was observed on the scaffolds, whereas histological sections and microCT showed, that cells, collagen and mineralization were mostly found at the scaffold edge. No differences between scaffold pore sizes were found, whereas for small pore size scaffolds produced form SF batch 1 substantially less mineralization was observed. MC3T3 were co-cultured with RAW 264.7 macrophages on 3D SF scaffolds of both pore sizes in mechanical loading bioreactors for 13 days in control or high calcium media. During culturing 5 times cyclic sinusoidal loading was applied for 30 minutes and mineralization was monitored with microCT. Biochemical assays showed, that MC3T3 osteoblasts differentiate more in co-culture with macrophages in high calcium media. Immunohistochemical staining on histological sections demonstrated the presence of macrophages within the scaffold after culture. No mineralization was observed on scaffolds cultured in control media, whereas in high calcium media increasing mineralization was monitored. Mechanical loading was seen to hinder osteoblast mineralization, whereas co-culture of macrophages accelerated mineralization rate on small pore size scaffolds. In conclusion co-culturing of macrophages with osteoblasts is a promising stimuli for osteoblast differentiation and mineralization enhancement, whereas loading did not enhance bone tissue formation on SF scaffolds.

Contents

Abbreviations

AA ascorbic acid

ALP alkaline phosphatase

ANOVA Analysis of variance

ARS Alizarin Red

BF Bright field microscopy

β-G β-glycerophosphate

BV/TV bone volume density

ECM extracellular matrix

FBS fetal bovine serum

HFIP hexafluoroisopropanol

IHC immunohistochemistry

IFN-γ Interferon-γ

L-Gln L-glutamine

MC3T3 osteoblast-like cell line

M-CSF macrophage-colony stimulating factor

MEM minimum essential medium

microCT micro-computed tomography

MSC mesenchymal stem cells

MSU mechanical stimulation unit

MΦ macrophage

NaCl sodium chloride

OB osteoblast

OPG osteoprotegerin

PBS phosphate buffered saline

PFA paraformaldehyde

PGA poly(glycolic acid)

PLA poly(lactic acid)

PLGA poly(lactiv-coglycolide)

RANK receptor activator of nuclear factor-κB

RANKL receptor activator of nuclear factor-κB ligand

RAW 264.7 macrophage-like cell line

RT room temperature

SEM scanning electron microscopy

SF silk fibroin

UPW ultra pure water

UTS ultimate tensile strength

Chapter 1

Introduction

Today there is the possibility in medicine to help injured or diseased people by implanting different types of grafts, being either from foreign species, so called xenografts, or from other individuals from the same specie - allografts. However, there will always be a foreign body reaction, which may result in the rejection of the implanted tissue or organ. For autografts, which are materials taken from the same individual from an other site, the repelling reaction is greatly reduced. It is still not an optimal solution, as the patient will undergo additional operation and therefore suffer further injury. Tissue engineering aims to provide new alternatives to autografts at least for tissues [46]. One approach is to extract cells from the patient, grow the needed tissue in a suitable atmosphere *in vitro* and implant it back into the patient. A brief illustration of the concept of tissue engineering is shown in figure 1.1. This new approach would also reduce immune body reaction, as the cells originate from the same patient and prevent transfer of viral contaminations.

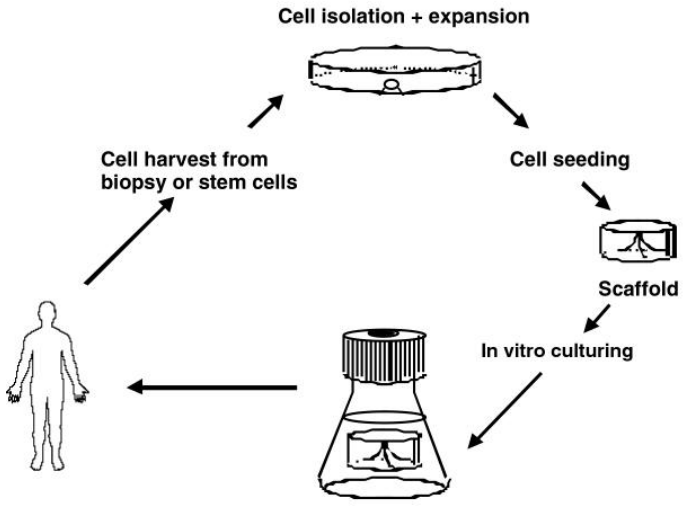

Figure 1.1: Concept of tissue engineering, image adapted from Stock *et al.* [46]

A lot of research focuses on tissue engineering of ligaments, heart valves, blood vessels, cartilage, bone and other tissues. After blood, bone grafts are the second most transplanted tissues [18]. Worldwide over 2.2 million bone grafting procedures are done annually in order to repair bone defects [18]. This shows the need for bone grafts and therefore the importance of tissue engineering in the area of bone tissue. In this project the focus is put on bone tissue engineering. The cells used to engineer bone-like tissue, need to be cultured in medium, that delivers nutrients and directs differentiation. As the final engineered tissue has to have a 3-dimensional (3D) architecture, the cells have to be grown on scaffolds, serving as 3D matrices. To give the cells a physiologic environment the cells are cultured in a normal cell incubator at 37°C. Cells seeded on a porous scaffold are generally cultured inside a bioreactor, holding the environmental factors as stable and constant as possible. In addition to preventing the environment, bioreactors can be designed to allow mechanical stimulation of the cells or allow a fluid flow. To obtain a suitable graft, suitable cells have to be chosen. Many researchers use the ability of mesenchymal stem cells (MSC) that are human or murine derived to differentiate along the osteogenic cell lineage into osteoblastic cells able to produce mineralized extracellular matrix (ECM). Preosteoblast cell lines show osteoblast-like behavior after differentiation and are investigated for bone tissue engineering. This project aims to tissue engineer bone-like tissue on silk scaffolds using a preosteoblast cell line while investigating the effect of co-cultured macrophages and the impact of cyclic mechanical stimulation of the cells during culture.

Chapter 2

Background

In this section first an overview on bone anatomy, bone cells and bone remodelling is given, then the background of mechanical stimulation of cells is presented. Furthermore available bioreactors for tissue engineering are reviewed and scaffolds in tissue engineering of bone-like tissue are described, while a special focus is put on silk fibroin scaffolds. At last micro-computed tomography (microCT) will be described and morphometric indices used in microCT analysis are discussed.

2.1 Bone

2.1.1 Bone anatomy

Bone has four main functions in the body, first it serves as structural support for mechanical action of soft tissues and general locomotion, second it protects vital internal organs, third it provides a protective site for the blood-forming tissue, the bone marrow where hematopoiesis takes place, and at last it is the mineral reservoir of calcium and phosphate for the body [4]. Bones can be categorized into three main groups according to their shape and size. Long bones, e.g. the femur or the tibia, which are long in one direction; short bones, which have around the same dimensions in all directions, such as the bones of the wrist and the ankle and as third class flat bones, such as the calvaria or the pelvis [4].

Bone tissue can be separated into two basic types, the compact or cortical bone and the trabecular or cancellous bone. Trabecular bone is made up of spicules, named trabeculae[4] and is intercalated with red bone marrow, where hematopoiesis occurs. Trabeculae are arranged in the way to provide optimal rigidity, thus they are aligned parallel along the main axis of compressive or tensile forces acting on the bone. Bones have varying amount of cortical and trabecular bone depending on their function. For

example long bones, such as the femur, which needs to withstand bending, shear and torsional forces, is consisted of a thick cortical layer with a medullary or central cavity (the diaphysis) and trabecular bone at the ends (the epiphysis) to transmit forces to the joints [4] (figure 2.1 (a)). During growth there is a cartilagenous structure containing chondrocytes between the diaphysis and the epiphysis of long bones, the growth plate, which is the place where the bone can grow by hypertrophy and subsequent ossification [4]. The outer bone surface is covered by the periosteum, and the inner bone surface by the endosteum. Both periosteal and endosteal surfaces are the place where constant bone remodelling takes place. An illustration of the anatomy of a long bone is shown in figure 2.1 (a).

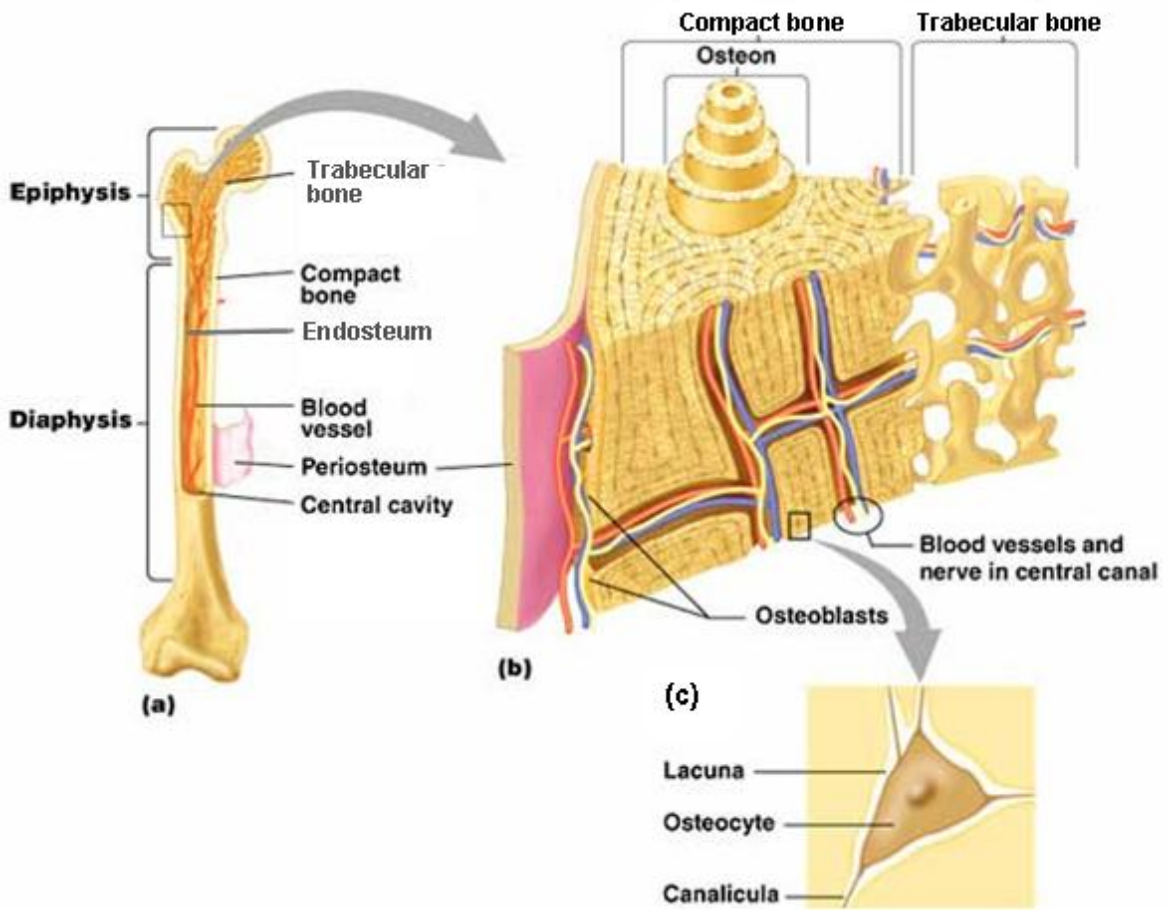

Figure 2.1: Schematics of bone anatomy: structure of a long bone (a), detailed structure of an epiphyseal segment (b), osteocyte location (c). Image adapted from http://www.personal.psu.edu/staff/m/b/mbt102/bisci4online/bone/bonestruc.jpg, with additional modifications

Bone is consisted of bone cells and intercellular material made up of an organic component including collagen fibers, mainly type I, small amounts of proteinpolysaccharides and glycosaminoglycans; and an inorganic component of calcium and phos-

phate forming mostly hydroxyapatite crystals [$Ca_{10}(PO_4)_6(OH)_2$] [41]. The mechanical properties of bone are a combination of the hardness of mineral crystals and the high tensile strength of the interwoven collagen fibers.

Bone tissue is further classified in woven or lamellar bone, due to the structural orientation of protein fibers and osteocytes, which are encapsulated, terminally differentiated bone forming osteoblasts. If collagen bundles and osteocytes are randomly oriented it is called woven bone, whereas these structures are aligned in layers, the bone is termed as lamellar. In cortical and lamellar bone exist further bone units, called osteons, which have concentrically cylindrical elements, building up the haversian system. In the center of osteons lies the haversian canal containing nerves and one or several small blood vessels, which supply osteocytes with nutrition. A diagram of the cortical and trabecular bone is shown in figure 2.1 (b). Other blood supply is found in the periosteum which contains an extensive blood vessel system or other nutrient arteries penetrating the bone tissue [4].

2.1.2 Bone cells

In bone several characteristic cell types can be found. On one hand there are osteoblasts, which synthesize new extracellular matrix on the bone surface and are able to mineralize it, thus build up new bone. And osteocytes, which are trapped osteoblasts in the bone structure, residing in a cavitiy, the lacuna. Osteocytes can communicate with each other through the connected channel system of the lacunae, the canaliculi [6] (figure 2.1 (c)). Both osteoblasts and osteocytes originate from mesenchymal stem cells, which are found in the bone marrow and can differentiate apart from osteoblasts and osteocytes also into bone lining cells, myocytes and chondrocytes [29]. On the other hand there are osteoclasts, multinucleated giant cells of hematopoietic origin. Hematopoietic stem cells, also found in the bone marrow, are progenitor cells of osteoclasts, monocytes/macrophages and other blood forming cells [42]. Both progenitor stem cell lines, mesenchymal and hematopoietic stem cells, are illustrated in figure 2.2. Osteoclasts form from preosteoclastic cells by maturation and fusion and are able to resorb bone matrix by excretion of enzymes and acidifying agents on the free bone surface. Osteoblasts produce two important cytokines, the receptor activator of nuclear factor-κB ligand (RANKL, also known as TRANCE) and the macrophage-colony stimulating factor (M-CSF), which are both essential for osteoclastogenesis. RANKL-RANK interaction induces the differentiation and maturation of preosteoclasts into matrix-resorbing osteoclasts via TRAF6 and further via the c-Src, JNK and NF-κB signaling pathways [48]. But, additionally to RANKL-RANK interaction, the soluble

factor osteoprotegerin (OPG) produced by osteoblasts can bind to RANKL, preventing an interaction with RANK, therefore inhibiting osteoclastogenesis [42].

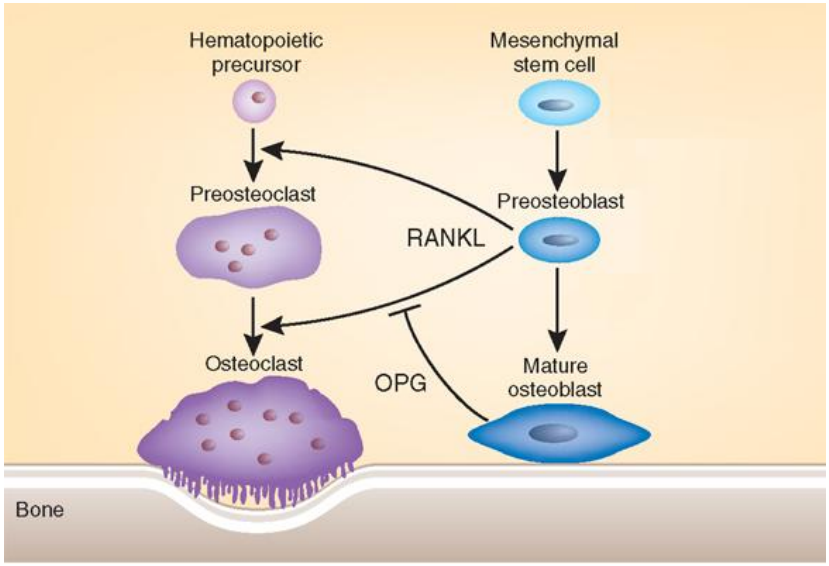

Figure 2.2: Illustration of the progenitor stem cells for osteoclasts and osteoblasts. Hematopoietic stem cells give rise to osteoclast, whereas Mesenchymal stem cells are the progenitor cells of osteoblasts. Image adapted from Goldring *et al.* [19], with additional modifications.

2.1.3 Bone remodelling

Skeletal bone is constantly remodeled by the dynamic process involving osteoclastic bone resorption and osteoblastic bone formation [3]. Thus, to ensure skeletal integrity as well as body's calcium metabolism, the actions of osteoblasts and osteoclasts have to be coordinated and kept in balance. If the rate of resorption exceeds the rate of formation, it is no longer balanced and leads to loss of bone mass as seen in diseases such as osteoporosis. The bone remodelling process includes first a recruitment of osteoclast progenitor cells and their differentiation into mature osteoclasts, then bone resorption by the multinucleated osteoclasts, and ends with the new bone formation and mineralization by osteoblasts at the same site. Macrophages have also been implicated at the remodelling site during the reversal phase, suggesting their function in removing eventual debris [23]. Figure 2.3 shows an illustration of the bone remodelling process.

Arron and Choi termed the new emerging field investigating the interactions between immune cells and bone cells osteoimmunology [3]. There is abundant evidence demonstrating this intimate relationship. For example, both immune and bone cells are generated in the same anatomical site, the bone marrow. It was demonstrated,

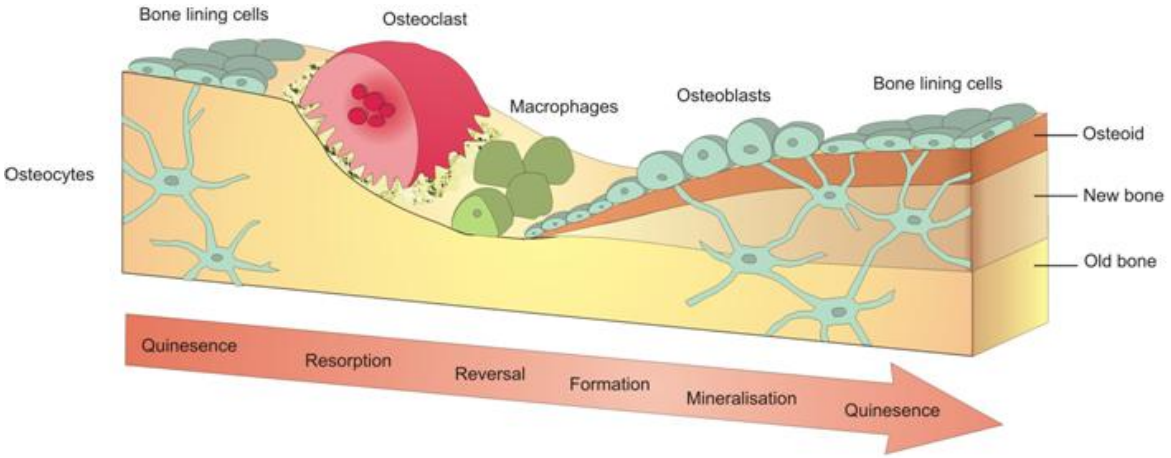

Figure 2.3: Illustration of the bone remodelling process. Bone lining cells uncover the bone surface and let osteoclasts to resorb bone matrix, macrophages remove debris and osteoblast start formation of new bone until inactive bone lining cells can recover the bone surface again. Image adapted from http://www.york.ac.uk/res/btr/Image%20Library/Bone%20remodelling.jpg, with additional modifications

that the molecule RANKL, apart from osteoblasts, is also expressed on activated T-cells, causing activation of osteoclasts through its receptor, receptor activator of nuclear factor-κB (RANK) on osteoclasts [53]. Besides RANKL expression T-cells secrete also the molecule Interferon-γ (IFN-γ) [48], which can bind to the IFN-γ receptor on osteoclast precursors inducing the destruction of TRAF6, preventing osteoclast maturation and bone resorption [3]. In addition, white adipose tissue produces several factors (adipokines), which interfere with the immune system and therefore also with the skeletal system. The immune system mainly interferes with bone resorption, while adipose tissue is mostly involved in the regulation of bone formation [8].

Chang *et al.* recently described a discrete population of F4/80$^+$ tissue macrophages, osteomacs, that intercalate amongst bone lining cells on resting endosteal and periosteal surfaces and form a canopy structure covering mature osteoblasts [10]. These osteomacs are defined by the expression of F4/80 and their anatomical location within osteal tissues [38]. It was shown, that the removal of osteomacs resulted in reduced osteoblast mineralization *in vitro* and depletion of osteoblastic bone forming surface *in vivo*, suggesting that osteomacs play an important role in bone dynamics by regulating osteoblast function [10]. A new bone remodeling model based on this observation was proposed, saying, that osteomacs stimulate osteoblast differentiation [36]. But they also allow osteoclasts to resorb bone matrix, as they unravel the canopy structure of bone lining cells and embedded osteomacs to give osteoclasts access to the bone surface

[36]. In pathological conditions osteomacs may even differentiate into osteoclasts, as they originate from common progenitors [36].

2.2 Mechanical stimulation of bone cells

According to Wolff's trajectorial theory, principal strain trajectories are responsible for the development and maintenance of trabeculae alignment in cancellous bone [5]. In Wolff's theory, and also with the knowledge, that children start to walk, thus applying forces to their bones, there is the main belief, that bone can sense applied forces and remodel the structure according to the main strain trajectories.

Duncan *et al.* [15] proposed the steps of mechanotransduction of external forces into bone remodeling. Mechanotransduction can be divided into four steps. The first step is the mechanocoupling, where mechanical load *in vivo* causes deformations in bone and thus stretches bone cells that lie in the lacunae, and produces fluid movement within the canaliculi, thus creating additional shear stresses on the surface of bone cells. In the second step biochemical coupling through different potential pathways transfer the mechanical signal on the cell level into intracellular biochemical signals. Following the third step, where transmission of the signal from the mechanosensor cell is communicated through cell interaction processes or secreted signaling molecules to other bone cells. At last the effector cells give their response by remodelling the bone structure. The final effects of mechanical loading are strongly dependent on the magnitude, duration and rate of applied load. It was found, that loading must be cyclic to have an effect for stimulating bone formation [15]. Despite these findings it is still not clear what kind of cells are able to sense mechanical stimulation and how the cells communicate a sensed stimulation to the effector cells, that a remodelling of bone takes place.

Several studies were investigating the effect of strains and pressure on bone cells and bone remodelling. For example Ozawa *et al.* [32] demonstrated, that continuously applied compressive pressure (CCP) inhibits the osteoblast cell line MC3T3 from differentiation and hinders mineralization of ECM. Whereas Jones *et al.* [27] showed, that mechanical loading of osteoblast-like cells by applying defined homogeneous strains in the physiological range, affects just periosteal derived osteoblasts. Application of high strains ($>$10000 μstrain) instead resulted in osteoblast de-differentiation [27]. One study focused on the biomechanical coupling pathway through analyzing the effect of chronic, intermittent strain on mechanosensitive cation channels in UMR-106.01 osteoblast-like osteosarcoma cells. This channel may act as a mechanotransducer for

the activation of bone remodeling by physical strain [14]. An *in vivo* study about applied strain and pressure on the calcaneus of potoroos and their effect of the underlying trabecular architecture showed, that trabecular alignment is established during growth and is not altered because of applied strains or disuse, the treatment could just influence the trabecular thickness, trabecular bone volume fraction or trabecular spacings, but not their orientation [5]. Palomares *et al.* [33] pointed out that depending on the mechanical stimulation selectively osteogenesis or chondrogenesis can be enhanced. Cyclic bending motion on femoral osteotomies of retired breeder sprague-drawler rats, showed to increase chondrogenesis over osteogenesis. In tissue engineering bone-like tissue was observed, that the structure of new built bone-like tissue is controlled by the geometry of the underlying scaffold [24]. Still, the definitive identification of the mechanosenitive cells and the pathways along which the signal is transduced to the effector cells is not yet done. There is no evidence, that only osteocytes and or osteoblasts are able to sense mechanical stimualtion.

2.3 Bioreactors used in tissue engineering

In the tissue engineering sector one tries to profit from the enhancement of osteogenesis by mechanical stimulation. The concept of mechanical stimulation is used in the construction of special bioreactors for culturing the tissue engineered grafts. Bioreactors provide an *in vitro* environment mimicking *in vivo* conditions for the growth of tissue substitutes, while creating a sterile environment for tissue culturing. Generally, normal static bioreactors, spinner flask bioreactors and perfusion reactors as well as bioreactors able to apply mechanical loading on the scaffold-cell constructs in different designs exist. Some bioreactors utilise just fluid flow, resulting in shear stress on the cells, or are even compressable to transmit mechanical force stimulation onto the cells seeded on the scaffold. Spinner flasks, where the cell seeded scaffolds are fixed and the nutrition media is spinned around in the flask, showed to give better cell distribution and matrix formation compared to static cell culture, on the other hand formation of an outer fibrous capsule around the scaffold was observed due to higher shear stresses caused by turbulent fluid flow [12]. To reduce the high shear stresses spinner flasks have been modified with wavy walls inducing smooth waves in the fluid flow [7]. Several perfusion system bioreactors have been constructed, where the perfusion of media through the scaffold helps to increase the cell migration into the scaffold interior, meanwhile the fluid flow creates a shear stress stimulation [12]. Freyria *et al.* [16] compared two different perfusion system bioreactors, the direct flow perfusion bioreactor and the free

flow reactor. While in the direct flow reactor the scaffold is fixed in place, in the free flow reactor the scaffold can be perfused freely in the bioreactor chamber. According to Freyria the free flow perfusion reactor is better compared to the direct flow, as the mass transfer of nutrients in the free flow system is more homogenous. Additionally, they determined an optimal flow rate and studied the influence of preculture duration in chondrocytes seeded on collagen scaffolds [16]. The mechanical stimulation is greatly dependent on the fluid flow magnitude and the stimulation pattern. Jaasma *et al.* [25] pointed out, that intermittent fluid flow caused greater stimulation on MC3T3-E1 osteoblast-like cells compared to continuous low flow fluid in perfusion bioreactors. A mechanical loading bioreactor was constructed and technically validated by Henri Hagenmüller, where on scaffold-cell constructs cyclic mechanical loading can be applied and a monitoring of mineralization can be conducted while maintaining a sterile environment [22]. In summary, the choice of the bioreactor and the possible mechanical stimulation pattern have a great impact on the cell growing and matrix mineralization of bone-like tissue samples.

2.4 Scaffolds for tissue engineering

To obtain a 3D graft, tissue engineering utilises scaffolds to build a suitable environment for cultured cells. Optimal scaffolds should have several physical and biochemical properties. Scaffolds should be porous and the pores should be interconnected to allow the cells to migrate into the whole scaffold after cell seeding. The scaffolds have to be designed to match the mechanical and surface features of normal biological tissue or at least should be stimulating for the cells. Many different materials have been used as scaffold materials, among those are natural occuring polymers, such as collagen, fibrin, agarose, hyaluronic acid, silk or synthetic polymers, e.g. poly(glycolic acid) (PGA), poly(lactic acid) (PLA), poly(lactiv-coglycolide) (PLGA) and others [43]. All these materials have characteristic mechanical and surface properties, which have to match the needed properties. Another very important aspect in choosing the material for scaffolds is the material's biodegradability and biocompatibility, as the scaffolds will be implanted into the body. An insufficent biocompatibility would lead to undesired immune reaction, which could hinder the incorporation into the body as a graft. Degradability is often requested, as the implant should be growing seamlessly into body's own structures, and therefore should be degradable by the bodies enzymatic digestion. Depending on the engineered tissue, the degradation process should be either fast or slow, matching the healing or regeneration process [9], as e.g. a scaffold

for bone-like tissue should degrade slowly to maintain the mechanical stability during ingrowth. The focus will now be led onto silk as a scaffold material, as it will be used in this project to support osteoblasts during bone-like tissue formation.

2.4.1 Silk fibroin scaffolds

Silks are protein polymers, which are spun into fibers by different lepidoptera larvae, such as silkworms, spiders, scorpions, mites and flies [1]. Silks specific functions are used by these species for building the cocoon capsular structure, prey caputre lines, lifelines or web construction. Each of these silks has a different amino acid composition. Especially silk from the domestic silkworm *Bombyx mori* has an old history in medical applications, as it has been used for centuries in surgery as sutures or in the textile production. The silk of the cocoon from *B. mori* is made of at least two major fibroin proteins, a light and a heavy chain, which build the core fibers. The fibrous fibroins are encased by a coat made up of sericin, which is a glue-like protein holding two fibroin fibers together. The fibroin compromises a crystalline portion and an amorphous region. The crystalline portion contains a highly repetitive amino acid sequence, made up of alanine-glycine repeats with serine or tyrosine [1, 9]. This repetitive sequence leads to the stability and the mechanical properties of silk fibers, as it can form a anitparallel β-sheet through hydrogen bonds between adjacent peptide chains [9]. Silk fibroin is found in two main structures, silk I or silk II. Silk I is made of random-coil and amorphous regions forming a water-soluble structure, whereas silk II has an antiparallel β-sheet insoluble structure [9]. Although virgin silk is a potential allergen, causing a type I allergic response, Wen *et al.* [52] showed, that only the sericin is responsible for an allergic response. To get a biocompatible suture or also scaffolds for tissue engineering, silk is processed to extract sericin from the biocompatible fibroin proteins. It was conducted a biocompatibility study of MSC on tissue culture plastic, collagen, polylactic acid (PLA) and silk fibroin films *in vivo* and *in vitro* [30]. The results of this study suggest that silk fibroin is biocompatible and induces similar or less inflammatory responses compared to tissue culture plastic, collagen or PLA [30]. Silk fibroin has very good mechanical properties, as it has a remarkable combination of strength and toughness. Table 2.1 shows a comparison of the mechanical properties of *B. mori* silk with sericin, extracted silk fibroin and bone, including values for ultimate tensile strength (UTS), elastic modulus and strain at break. The mechanical properties suggest, that regenerated (purified) silk fibroin is a suitable scaffold material for bone tissue engineering, as it has similar or enhanced mechanical properties compared to bone.

Material	UTS [MPa]	Modulus [GPa]	Strain at break	Ref.
B.mori silk	500	5-12	19	[35]
B.mori silk fibroin	610-690	15-17	4-16	[35]
Bone	160	20	3	[20]

Table 2.1: Mechanical properties of silk containing sericin, silk fibroin and bone [1]. Listed are the values for the ultimate tensile strength (UTS), the elastic modulus and the strain at break. All values are adapted from the cited references.

There are at least three different fabrication methods to obtain porous silk fibroin scaffolds. All of them contain a first silk purification step, where the sericin proteins are extracted from silk fibroins. Then either freeze-drying, gas foaming or porogen/leaching methods can be used [31]. All these methods contain a final step, at which the silk structure is converted from the soluble silk I configuration into the stable and insoluble silk II structure for finishing the scaffolds. The different methods employ various factors to influence the pore size, interconnectivity as well as the surface structure of the scaffolds. In this project the porogen/leaching method will be used to produce silk fibroin scaffolds. This method can be further categorized depending on the porogen and the solvent used in the process. As Porogens either NaCl particles [31] or paraffin globules [49] are used with subsequent porogen leaching in water or hexane to unoccupy the pores in the scaffold. The solvent used in the leaching fabrication method causes a huge difference in scaffold properties, therefore one differentiates between all-aqueous or solvent (e.g. Hexafluoroisopropanol (HFIP)) derived procedures [28]. The comparison of silk fibroin scaffolds prepared by all-aqueous or solvent derived methods unravels a clear difference in faster cell ingrowth and much faster scaffold degradation time of the former ones. The choice of the solvent can be used to tailor scaffolds to the needed degradation times, such as a fast degrading water-based scaffolds suit well for drug releasing applications, whereas slow degrading HFIP derived scaffolds fit best for long-term bone regeneration [51].

2.5 Micro-computed tomography

Micro-computed tomography (microCT) is a non-destructive technique able to provide 3-dimensional images of the internal structure of an object [45]. In a microCT scanner a micro-focus X-ray tube emits X-rays. The X-ray beam passes a collimator and filters to narrow the energy spectrum and then pass the sample, where a material dependent amount of energy gets absorbed. The attenuated beam is then detected by

a two-dimensional CCD array, recording projections of the sample [45]. To get a 3-dimensional image, the sample is rotated over 180° taking multiple projections, which can be reconstructed back into a 3D image of the object [45]. Morphometric indices calculated from microCT data are used to access structural properties of cortical and trabecular bone. Standard morphometric indices used are bone volume (BV), which is the volume of the minerlized voxels in the analyzed volume of interest (VOI); bone volume density (BV/TV), which is the percentage of bone volume per total analyzed volume; bone surface (BS), which is computed using a triangularization of the object surface; specific bone surface or bone surface to volume ratio (BS/BV), which relates the bone surface to the total bone volume [45]. There are also indices specifically for trabecular bone as mean trabecular thickness (Tb.Th) or mean trabecular number (Tb.N), which are both based on a sphere fitting model [45]. The porosity of an object is characterized computing the connectivity density (Conn.D), which describes the number of possible paths from one side of the object to the opposite side and is based on the Euler number [45]. There is an other index, which describes the plate-rod characteristics of trabecular bone, which is called structure model index (SMI). The SMI is a value between 0 and 4, whereas 0 represents perfect plates, 3 perfect rods and 4 perfect spheres [45]. MicroCT analysis are used in this study to investigate SF scaffold morphology and to monitor osteoblast mineralization on SF scaffolds over culture time.

Chapter 3

Experimental plan

First of all silk fibroin scaffolds suitable for tissue engineering of bone-like tissue were produced according to a protocol using the Hexafluoroisopropanol (HFIP)-based salt leaching method. Scaffolds with two different pore sizes were produced using porogens of sizes between 112-224 μm or 224-315 μm diameter, respectively. The scaffolds were characterized using microCT analysis and scanning electron microscopy (SEM) investigations.

Preliminary experiments with MC3T3 osteoblasts in 2D tissue culture plates were performed to investigate the optimal cell density, the culturing time required and the optimal culture conditions for this cell line to produce mineralized ECM. Culture conditions were tested using different media; normal maintenance medium as well as two different osteogenic media. MC3T3 osteoblasts were cultured for different time periods and then analyzed for collagen production, mineralization, DNA content and alkaline phosphatase (ALP) activity.

Subsequently, the results from 2D experiments were translated into 3D to investigate the osteoblast mineralization on silk fibroin scaffolds over time. Firstly, an experiment using the most simple bioreactors, static bioreactors, was conducted. The optimized cell density of 2D investigations was upscaled to 3D and the best osteogenic media was used to tissue engineer bone-like structure on SF scaffolds. MC3T3 osteoblasts were cultured using two different pore sized scaffolds generated with different SF batches to investigate possible differences. Mineralization was monitored over time with non-destructive microCT measurements. After culturing the scaffolds were analyzed for collagen production, mineralization, DNA content and ALP activity. Scaffolds were also fixed and examined by SEM and histology.

Furthermore a co-culturing experiment using MC3T3 osteoblasts and RAW264.7 macrophages [39] was done to study the effect of macrophages on osteoblast mineralization in 3D on SF scaffolds. The co-culturing experiment was combined with mechanical

load-induced stimulation of the cells on the scaffolds using an established mechanical stimulation unit (MSU) and specially constructed bioreactors [22]. Mechanical stimulation amplitutde, frequency and duration was chosen to similar experiments carried out with the MSU (unpublished data). Cells were cultured in elevated extracellular calcium media as a physiologic anabolic signal to stimulate mineralization in vitro [10]. After culturing the scaffolds were analyzed for DNA content and ALP activity. Futhermore cell distribution, collagen production and mineralization on the scaffolds was demonstrated by histological sections. Immunohistochemical analysis was also done to show the survival of macrophages in co-culture in the SF environment.

Chapter 4

Materials and Methods

4.1 Materials

Ultra pure water (UPW) (Sartorius stedim biotech, Goettingen, Germany) was always used if stated water. Fetal bovine serum (FBS), Normal goat serum (NGS), Minimum Essential Medium α (αMEM), antibiotic-antimycotic solution named penicillin/streptomycin/fungizone (P/S/F), trypsin/ EDTA (0.25%) were form Gibco, Invitrogen (Carlsbad, CA). Dimethyl sulfoxide (DMSO), Ethanol, Sodium chloride (NaCl) and Tris(hydroxymethyl)-aminomethan (Tris base) were from Fluka (Buchs SG, Switzerland). L-Ascorbic acid 2-phosphate sesquimagnesium salt hydrate (AA), Accustain Eosin Y solution (Eosin), β-Glycerophosphate (β-G), Mayer's Hematoxylin solution (Hematoxylin), Methanol and Paraformaldehyde (PFA) were from Sigma-Aldrich (St. Louis, MO, USA). PBS tablets were from Medicago (Uppsala, Sweden). 10x Tris-buffered saline contained 0.5M Tris base, 9 wt% NaCl in UPW, the pH was adjusted with hydrogen chloride (HCl) to 7.4. Absorbance and fluorescence measurements were performed on a microplate reader, Tecan Plate reader infinite 200 (Männedorf, Switzerland).

4.2 Silk fibroin scaffold preparation

Silk cocoons from the silkworm *Bombyx mori* (supplied by Trudel Inc., Zürich, Switzerland) were cut in half, silk worms were removed and the cocoons were cleaned from debris and other contaminations. Further cut pieces of the cocoons were boiled in a sodium carbonate (Na_2CO_3 anhydrous, Fluka) solution to extract the sericin proteins from the remaining silk fibroin material. The silk fibroin was dried completely, further disolved in a lithium bromide (Fluka) solution and heated up to 55°C for one hour. Lithium bromide salt was removed from the silk fibroin solution by dialysis (Pierce,

Rockford, US) against water. After filtering the solution through a 5 μm pore size filter (Sartorius AG, Goettingen, Germany), the silk fibroin solution was frozen at -80° C for subsequent lyophilization (Christ, Osterode, Germany).

1,1,1,3,3,3-Hexafluoro-2-propanol (HFIP, Sigma) was used to disolve the lyophilized silk to get a viscous silk solution. Sodium chloride particles with sizes between 112-224 μm or 224-315 μm used as porogens were prepared in a teflon mold. The viscous silk/HFIP solution was poured over the porogens to form a mixture. The solvent was let to evaporate and the silk/porogen composite was immersed in methanol to induce a protein conformational transition of the fibroin from silk I into silk II, a water-insoluble β-sheet. The salt porogens were removed by salt leaching when immersing the composite in water. The dried scaffolds were cut and punched out to get scaffolds of 5 mm in diameter and a heigth of 2 to 3 mm.

4.3 Mammalian cell culture

4.3.1 Osteoblast cell line MC3T3

MC3T3-E1 Subclone 14 osteoblast precursor cell line was a gift from Prof. Franz Weber (University Hospital, University of Zürich), originally obtained from American Type Culture Collection (ATCC, Rockville, MD, USA). MC3T3-E1 is a clonal osteogenic cell line derived from newborn mouse calvaria showing an osteoblast-like phenotype [47]. Subclone 14 is a subpopulation of the original heterogenous MC3T3-E1 cell line with a high differentiation and mineralization potential *in vitro* [50]. The cells are routinely grown in complete maintenance medium (Minimum Essential Medium (MEM) alpha (without AA) with 10% FBS) in an incubator at 37°C with 5% CO_2 in air atmosphere. After reaching confluence the cells were trypsinized (0.25% Trypsin-EDTA solution) and split routinely using subcultivation ratios of 1:6 to 1:8. The media was changed every 2 to 3 days.

4.3.2 Macrophage cell line RAW 264.7

RAW 264.7 macrophage-like cell line was a gift from Dr. Vera Ripoll (MRC, UK), originally obtained from ATCC. The cell line was derived from murine tumors induced by Abelson leukemia virus, that exhibit macrophage properties [40]. The cell line was routinely grown in RPMI media (Gibco) with 5% heat-inactivated FBS (HI-FBS), 1% P/S/F and 1% L-Gln in bacteriological plates in an incubator at 37°C with 5% CO_2 in air atmosphere. The cells were split using a subcultivation ratio of 1:10 to 1:20 every

2 to 3 days.

4.3.3 Cell line storage

Low passage numbers of both cell lines were stored in liquid nitrogen in freezing media containing 10% DMSO in FBS. Thawing cells previously stored in liquid nitrogen was done rapidly at 37° C and fast removal of the DMSO by suspension with complete maintenance media.

4.3.4 Experimental culturing conditions

2D culture of MC3T3 osteoblasts

Low passage numbered MC3T3 osteoblasts were trypsinized and cell number were assessed using a Neubauer hemocytometer (Brand, Wertheim, Germany). The experiment was set up to use 3 different cell concentrations, $1.2\text{x}10^4$, $2.4\text{x}10^4$ and $5.2\text{x}10^4$ cells/well in 24-well plates. 6 different osteogenic and control media were used, all media contained additionally 10% FBS and 1% P/S/F and further supplements, see table 4.1.

Name	Media	Supplements
1	complete maintenance media	
2	BGJb (Fitton-Jackson mod.)	1% L-Gln
3	BGJb (Fitton-Jackson mod.)	1% L-Gln, 50μg/ml AA, 10mM β-G
4	MEM alpha (standard, with AA)	
5	MEM alpha (standard, with AA)	50μg/ml AA
6	MEM alpha (standard, with AA)	50μg/ml AA, 10mM β-G

Table 4.1: Media nomenclature

Medium was changed 3 times a week. Every cell concentration and media was done in triplicate. Two experiments were conducted, one for 16 and 26 days and one for 18 and 28 days.

3D culture of MC3T3 osteoblasts on SF scaffolds in static bioreactors

SF scaffolds were autoclaved and presoaked in PBS and then in maintenance medium for at least 1 hour. Cell density used was in accordance to 2D culture, the lowest seeding concentration. Cell number per scaffold was adjusted according to the scaffold height and an average cell height of 2.4 μm [2]. Due to different scaffold

heights this resulted in cell numbers of 1-1.7x10^6 cells per scaffold. SF scaffolds were placed in static bioreactors, cells seeded and let to adhere for 1 hour. Then the scaffolds were fixed with a clamp screw, the chamber filled with 5ml number 4 media and the cap srewed on partly to still allow gas exchange. At day 3 the medium was changed to number 3 media. Medium was exchanged 3 times per week.

3D co-culture of MC3T3 osteoblasts and RAW 264.7 macrophages on SF scaffolds in mechanical loading bioreactors

SF scaffolds were glued (Heraeus Kulzer, Wehrheim, Germany) into mechanical loading bioreactors and dry-autoclaved together with the bioreactors. Scaffolds were prewetted with number 4 media for at least 1 day. MC3T3 were seeded at 1.2x10^6 cells/scaffold and let adhere for 1 hour. Additionally 1.8x10^5 RAW 264.7 cells/scaffold were co-seeded and let to adhere for another 30 minutes. Each bioreactor was filled with 5ml MEM (MEM+GlutaMAX (Gibco)) containing either vehicle control HEPES or 4mM $CaCl_2$ (Prolabo). The bioreactors were closed and cultured in an incubator at 37°C with a 5% CO_2 in air atmosphere.

4.3.5 Cell fixation

After culturing period media was aspirated and the cells in well plates or on scaffolds were washed 3 times with PBS and subsequently fixed with 4% PFA. Cells in 2D culture were fixed for 30 minutes at room temperature (RT), whereas on scaffolds they were fixed for 24 hours at 4°C.

4.4 Mechanical loading

Mechanical loading on scaffolds seeded with cells was done using specially designed bioreactors able to mechanically load scaffolds with a mechanical stimulation unit (MSU). The bioreactors and the MSU were designed and technically validated by Henri Hagenmüller [22]. The bioreactors combine monitoring using micro-computed tomography (microCT) and direct mechanical loading of scaffolds [21]. The loading device was suited in a laminar flow hood to maintain the sterile environment in the bioreactors during loading. The bioreactor chambers were closed during the whole experiment with a tube allowing media exchange. Gas exchange was enabled by opening the spring-loaded part during mechanical stimulation or in the incubator, while no gas exchange was allowed during microCT scanning. The bioreactors were designed to fit two scaffolds at a time with only one of them loaded. Bioreactors were loaded using a scaffold

detection trigger level of 0.1N, a cyclic sinusoidal loading pattern with a frequency of 1 Hz and a loading amplitude of 5% of the scaffold height for 30 minutes.

4.5 Micro-computed tomography

For all microCT measurements a microCT40 imaging system (Scanco Medical, Bassersdorf, Switzerland) was used. SF scaffold characterization was done by scanning dry scaffolds in a tube of 12.3 mm diameter using an energy of 40 kVp, at an intensity of 180 μA, an integration time of 200 ms and a two times frame averaging in a high resolution mode, which resulted in a nominal resolution of 6 μm. Scaffolds cultured in static bioreactors were scanned in bioreactors (diameter 36.9mm) using an energy of 40kVp at an intensity of 180 μA, an integration time of 200ms and a two times frame averaging in a medium resolution mode resulting in a nominal resolution of 36 μm. Mechanical stimulated cells on scaffolds were measured in MSU bioreactors (diameter 36.9mm), using a X-ray beam with energy 40 kVp, 180 μA intensity, an intergration time of 200ms, 2 times frame averaging in a high resolution mode, giving a nominal resolution of 18 μm. A Gaussian filter was used to suppress noise. Image processing was done by defining a volume of interest (VOI) using GOBJ masks as contours. Image analysis was done with the standard analysis software SAX using in-house scripts SCAF for dry scaffolds and BIOR for cell seeded scaffolds. In all cases a filter width of 0.8 and a filter support of 1 was chosen. The lower threshold was set for dry scaffolds at 45, for scaffolds in static bioreactors to the standard BIOR value of 165 whereas for scaffolds cultured in MSU bioreactors a lower threshold of 215 had to be used to separate artefacts from the actual mineralization. Characteristic morphometric indices normally used in bone analysis were calculated to evaluate dry scaffolds. These values were scaffold volume (in analogy to bone volume (BV)), scaffold surface (BS), scaffold volume density (BV/TV), scaffold surface to volume ratio (BS/TV), wall thickness and wall number, structure model index (SMI) and the connectivity density (Conn.D). Bone volume density (BV/TV) of cell seeded scaffolds was evaluated to monitor mineralization over time.

4.6 Scanning electron microscopy

SF scaffolds seeded with cells were PFA fixed and additionally fixed with 2.5% Glutaraldehyde solution in 0.1M cacodylate buffer (pH 7.4) for 4 hours, rinsed with 0.1M cacodylate buffer and postfixed with 0.1% aqueous osmium tetroxide in 0.1M cacody-

late buffer for 90 minutes in the dark. After a further rinse with 0.1M cacodylate buffer, the samples were dehydrated in a series of rising ethanol concentration, frozen in pure ethanol at -80°C and lyophilized for 1.5 days. Lyophilized samples and air-dried SF scaffolds without cells were mounted with carbon sticker onto SEM sample holders, gold sputtered and imaged in a scanning electron microscope (SEM) (CamScan, Cambridgeshire, UK) using a working distance of 35mm and a high voltage of 20kV.

4.7 Biochemical analysis

4.7.1 Alizarin Red assay

PFA fixed cells or scaffolds were stained with 40mM Alizarin Red solution (Fluka) (pH 4.0 adjusted with Ammonium hydroxide) at RT with slight shaking for 30 minutes. The solution was aspirated and the cells were washed with UPW until no more color leaked out. The cells/scaffolds were air-dried before bright field (BF) images were taken. For qualitative analysis of the stained deposits the staining was disolved in 5% perchloric acid at RT with slight shaking for 15 minutes. A colorimetric analysis was performed by measuring the absorbance at 405nm.

4.7.2 Alkaline phosphatase activity assay

A lysis solution of 0.2% (v/v) Triton-X 100 (Fluka) and 5mM $MgCl_2$ (Magnesium chloride hexahydrate, Fluka) in UPW was added to the cells/scaffolds. Cells were disintegrated by pipeting the solution up and down and scaffolds were disintegrated with steelballs and a Minibead beaterTM (Biospec, Bartlesville, OK). After centrifugation (300g, 10min) the supernatant was used to perform the assay by adding 0.75M 2-amino-2-methyl-1-propanol (AMP, Sigma) buffer solution and 10mM substrate solution p-nitrophenylphosphate (p-nitrophenylphosphate disodium hexahydrate, Fluka) and let to react until color developed. The reaction was stopped by adding 0.2M sodium hydroxide (Hänseler, Herisau, Switzerland). The absorbance was read at 405nm. P-nitrophenol concentration [mM] was calculated using a standard curve generated with p-nitrophenol standards measured at the same time as the samples.

4.7.3 Calcium assay

Scaffolds were immersed in 5% (v/v) trichloroacetic acid (TCA, Hänseler) in UPW solution and disintegrated with steelballs and a Minibead Beater and incubated at RT for 48 hours. The samples were centrifuged (3000g, 10min) and the supernatant was

used to perform the assay. Standards with defined calcium concentration were used as references. The colorimetric calcium assay kit Calcium CPC from Rolf Greiner Bio-Chemica (Flacht) was used according to the manufacturer's protocol. The absorbance was read at 575nm.

4.7.4 DNA assay

For the DNA assay the same supernatant containing lysis solution and disintegrated scaffolds after centrifugation used for the ALP activity assay was taken. The DNA content was determined using the Quant-iT^{TM} PicoGreen® dsDNA Quantitation Kit (Invitrogen). In a black microtiter plate for fluorescent reading (Nunc) standards and sample wells were prepared according to the manufacturers protocol. PicoGreen reagent solution was added in the dark and incubated for 3 minutes. Fluorescence intensity was read with a microplate reader using an excitation of 480nm and an emission of 520nm.

4.7.5 Sirius Red assay

PFA fixed cells were stained with 1mg/ml Sirius Red solution (Direct Red 80, ABCR, Karlsruhe, Germany) in saturated picric acid (Fluka) and incubated at RT with slight shaking for 18 hours. The solution was aspirated, the cells/scaffolds were washed in UPW until no more color leaked out and samples were air-dried. Bright field light microscopy images were taken. To semi-quantitatively access collagen, the red staining was dissolved in a 1:1 mixture of methanol and 0.2M NaOH in UPW for 20 minutes. The absorbance of the resulting solution was measured at 490nm using a microplate reader.

4.8 Histology

PFA fixed scaffolds were embedded in Paraffin using an automatic Tissue Processor (Medite Medizintechnik AG, Nunningen, Switzerland) running a cycle of increasing ethanol concentrations for dehydration, Xylol and Paraffin over night. The Paraffin infiltrated samples were oriented and embedded in a paraffin block using an embedding system. Serial sections of 5 μm thickness from the top and from the middle part of the scaffolds were cut using a rotary microtom HM 355 S (Microm, Walldorf, Germany), placed on positively charged glass slides (Menzel Gläser, Braunschweig, Germany) and dried at 37°C.

4.8.1 Dewaxing and Rehydration of embedded sections

The Paraffin embedded sections were dewaxed and rehydrated for further staining procedures. Slides were heated for 1 hour in an oven at 60°C to melt the paraffin and adhere the sections to the slides. Subsequently the slides were incubated sequentially in batchs of Xylene, 100% Ethanol, 90% Ethanol, 70% Ethanol and UPW for 5 minutes each.

4.8.2 Hematoxylin and Eosin (H&E) Staining

Dewaxed and rehydrated sections were stained with Mayer's Hematoxylin, washed in tap water to mature Hematoxylin staining, stained in Eosin with subsequent Eosin maturation baths of 95% Ethanol and 100% Ethanol, followed by Xylene baths. Cover slides were directly mounted using permanent mounting media (Richard-Allan Scientific, Kalamazoo, USA).

4.8.3 Von Kossa Staining

Dewaxed and rehydrated sections were stained with 1% silver nitrate ($AgNO_3$, Sigma) solution and exposed to UV light for 45 minutes. Silver nitrate solution was subsequently removed and the sections were washed with UPW. The sections were then incubated in 5% sodium thiosulfate ($Na_2S_2O_3$, Sigma) for 2 minutes. After additional UPW washs the sections were air-dried and mounted using permanent mounting media.

4.8.4 Immunohistochemical staining for F4/80$^+$ macrophages

Immunohistochemical staining was performed using an immunoperoxidase technique with diaminobenzidine (DAB) as chromogen. Sections were deparaffinized and rehydrated followed by antigen retriveal. Antigen retrieval was done by incubating sections with 0.37% trypsin (Biocare Medical, Concord, USA) at RT for 10 minutes. All following dilutions were performed using Tris buffered saline unless stated otherwise. Firstly, non-specific binding blockade was performed using a serum block (10% FBS plus 10%NGS) for an hour at RT. Sections were then incubated with either the primary antibody F4/80 (AbD Serotec, Oxford, UK) or the isotype control rat IgG2b (AbD Serotec) at RT for an hour. A 5 minutes wash using TBS was carried out here and between each following step. Section were subsequently incubated with 3% hydrogen peroxide (Acros Organics) for 30 minutes to block endogenous peroxidase activity. Sections were washed and incubated with a biotin conjugated goat anti-rat IgG F(ab')$_2$-B

(Santa Cruz Biotechnology) secondary antibody for 30 minutes. Then, sections were incubated with Streptavidin-Horseradish peroxidase (HRP) (AbD Serotec, Kidlington, UK) solution for 30 minutes. Finally sections were developed using DAB chromogen (Dako, Glostrup, Denmark) according to the manufacturer's protocol for 10 minutes. All samples were counterstained with Mayer's Hematoxylin and mounted using permanent mounting media.

4.8.5 Sirius Red staining

Dewaxed and rehydrated scaffold sections were stained with Sirius Red solution (see 4.7.5) and incubated for 18 hours, counterstained with Hematoxylin, air-dried and mounted using permanent mounting media.

4.8.6 Alizarin Red (ARS) staining

Dewaxed and rehydrated scaffold sections were incubated with 40mM ARS solution for 30 minutes, air-dried and mounted using permanent mounting media.

4.8.7 Image acquisition

Bright field light microscopy images were taken with an inverted microscope (Zeiss) or an upright microscope (Zeiss) using as software Axiovision and an AxioCamMR color camera.

4.9 Statistical analysis

Statistcally significant differences were determined using one-way ANOVA (Analysis of Variance) test for repeated measurements with a Bonferroni post-hoc test or an unpaired t-test where applicable using Prism (GraphPad, USA). A p-value of < 0.05 (*) was deemed statistically significant, $p < 0.01$ (**) as very significant and $p < 0.001$ (***) as extremely significant. Data was represented as mean $\pm$ SEM (standard error of mean) if multiple measures were available.

Chapter 5

Silk fibroin scaffold characterization

3D Silk fibroin scaffold constructs for generating tissue engineered bone-like tissue were produced according to the porogen/leaching method using NaCl crystals as porogens. Two different sizes of NaCl crystals, 112-224 μm and 224-315 μm in diameter were used to obtain scaffolds with smaller and larger pore sizes. SF scaffolds made from three different silk fibroin batches, produced the same way, were compared to determine whether there was variability between batches. SF scaffolds were characterized using scanning electron microscopy (SEM) and micro-computed tomography (microCT).

5.1 Results

5.1.1 Silk fibroin scaffold topography

The topography of SF scaffolds was analyzed with SEM. Secondary electrons were detected as they originate from the top few nanometers of the sample and thus contain a topographic information. SF scaffolds were non-conductive samples, which had to be coated with Au to obtain a conductive sample beforehand. SEM is operated in high vacuum, therefore the scaffolds had to be dry during measurement. SEM images of SF scaffolds of the two different pore sizes produced from two or three different SF batches at a magnification of 50x and 100x were shown in figure 5.1.

SEM images clearly demonstrated pores within SF scaffolds (figure 5.1). The pores within each scaffold varied in diameter as well as not being completely round but rather squared, as expected since octahedral NaCl crystals were used as porogens. Overall a difference in pore size could be seen between scaffolds produced from smaller NaCl crystals compared to larger ones (figures 5.1 A, B vs. E-G). Comparing the two SF batches in smaller pore size scaffolds it seemed, that batch 2 had rather smaller pores compared to batch 1, although considering just the darker part of image 5.1 B, there

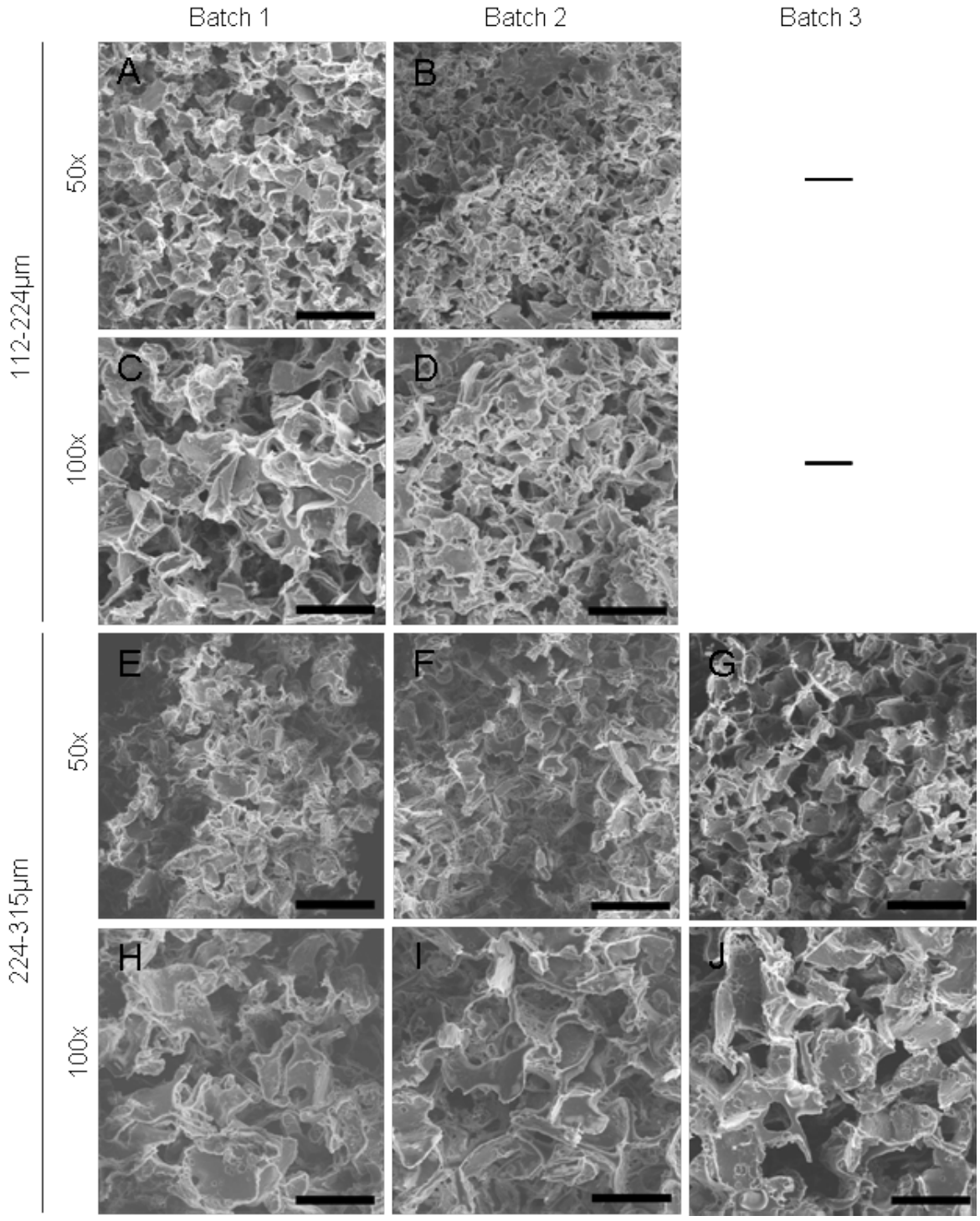

Figure 5.1: SEM images showing the surface morphology of SF scaffolds. Scaffolds with pores made from porogens with 112-224 μm (A-D) and 224-315 μm (E-J) diameter made from two or three different silk fibroin batches are shown in different magnifications. The scale bar represents 500 μm in 50x magnified images (A, B, E-G) and 250 μm in 100x magnified images (C, D, H-J).

seemed to be no difference in pore sizes. In large pore size scaffolds all 3 SF batches showed similar pore sizes (figure 5.1 E, F, G and H, I, J). The walls of the SF strucutre in the scaffolds were mostly smooth, with sometimes few holes or deepenings in all of the scaffolds. The wall thickness of the SF walls could be seen on pores, which were cut perpendicular to the imaging axis. Comparing the wall thickness of open pores of all scaffolds by eye, for small and large pore size scaffolds of all SF batches the wall thickness seems to be in a similar range.

5.1.2 Silk fibroin scaffold morphology

To study the morphology of SF scaffolds of smaller and larger pore sizes microCT scanning of dry scaffolds was conducted. The scanning parameters were set to reach a nominal resolution of 6 μm. MicroCT images of silk fibroin structure and images showing the void volume modelling of both scaffold types made from different SF batches are presented in figure 5.2. The void volume modelling images were made by fitting globules with the size of the pore diameter into the pores. The SF wall thickness as well as the pore sizes are color-coded.

All microCT images of the silk fibroin structures (figure 5.2) showed homogenous pore distributions and similar wall thickness, with just a few expectations, where the wall thickness was colored redish to be thicker. By eye no difference in wall thickness could be seen between large and small pore size scaffolds, but it needed to be considered, that the color-code did not have the same scale. Therefore it seemed, that large pore size scaffolds had slightly thicker SF walls than small pore size scaffolds (figure 5.2 left column). The void volume images showing modelled pore sizes were more inhomogenous (figure 5.2 right column). There were a few larger globules present in all scaffolds indicating larger pores. Still, with considering the different color scales the gloubles in small or large pore sized scaffolds, respectively, seemed to be in a similar range for all SF batches.

The evaluation of the measured microCT images provided values of different morphometric indices usually used to characterize trabecular bone. These parameters could also be used to characterize SF scaffold morphology. Therefore morphometric indices as scaffold volume, scaffold surface, scaffold volume density, scaffold surface to volume ratio, wall thickness, wall number, structure model index and connectivity density were calculated from microCT data of SF scaffolds. As no differences between SF batches within the same pore sizes in both small and large pore sizes were found, morphometric indices were averaged for small and large pore sized scaffolds, respectively. Values for scaffold volume, scaffold surface, scaffold volume density, scaffold surface to volume

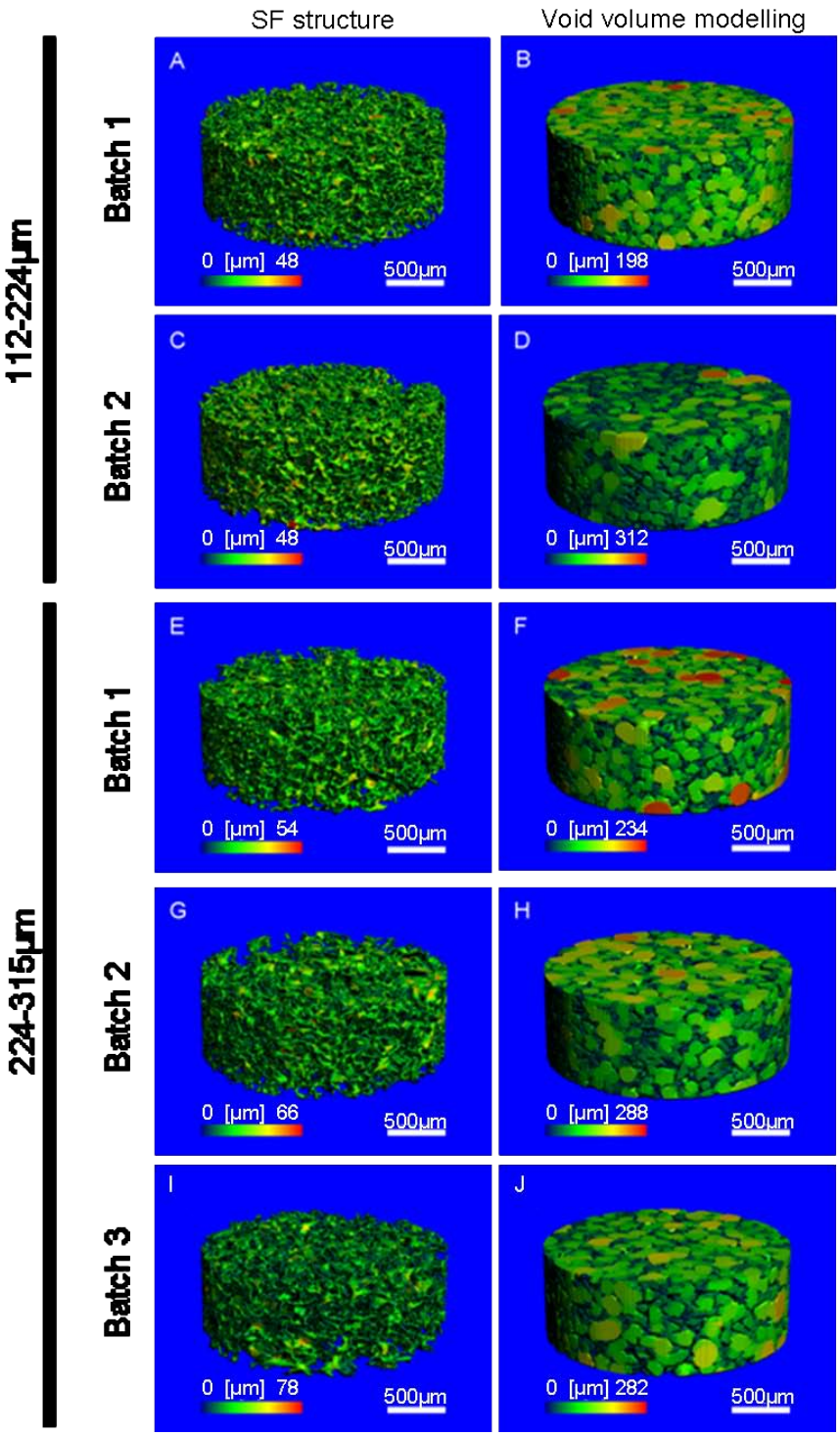

Figure 5.2: MicroCT images representing silk fibroin structure (left column) and void volume modelling (right column) of two scaffold types produced with porogens with 112-224 μm (A-D) or 224-315 μm (E-K) in diameter and made from three different SF batches. Color scale represents the thickness of SF walls (left) or size of fitted globules in the pores (right). Scale bars are shown in the images.

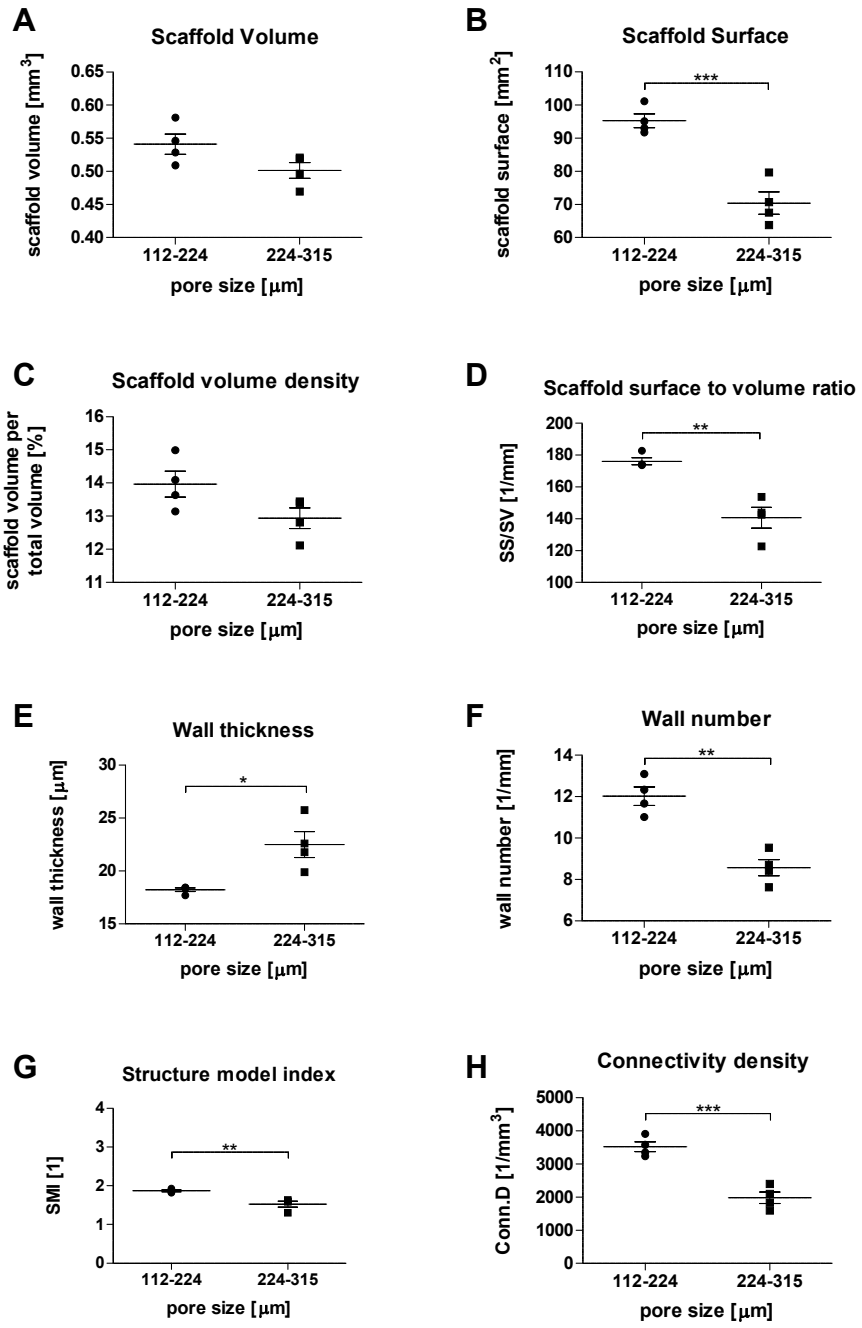

Figure 5.3: Standard structure analysis of microCT images from dry SF scaffolds was used to calculate morphometric indices. Scaffold volume (A), scaffold surface (B), scaffold volume density (C), scaffold surface to volume ratio (D), wall thickness (E), wall number (F), structure model index (G) and connectivity density (H) are shown of scaffolds produced with 112-224 μm or 224-315 μm NaCl porogens. Data represent mean value of n=4 scaffold $\pm$ SEM. Statistical differences are analyzed with an unpaired t-test, where a p-value < 0.05 (*) represents statistically significant, $p < 0.01$ (**) very significant and $p < 0.001$ (***) extremly significant differences.

Pore size	scaffold	Porosity [%]	Mean porosity ± SD[%]
112-224 μm	1	86.9	
	2	86.4	
	3	85.0	
	4	85.9	86.0±0.8
224-315 μm	1	86.6	
	2	87.9	
	3	87.2	
	4	86.6	87.1±0.7

Table 5.1: Porosity of SF scaffolds produced with porogens of diameters between 112-224 μm or 224-315 μm are listed. Mean porosity values are calculated from 4 different scaffolds (n=4) of one pore size. There is no statistically significant difference between the two pore sizes using an unpaired t-test.

ratio, wall thickness, wall number, structure model index and connectivity density averaged over 4 scaffolds each (n=4) are shown in figure 5.3.

The scaffold volume was for both pore sizes in a similar range and not significantly different (figure 5.3 A), as well as the scaffold volume density (figure 5.3 C). There were extremely significant differences between scaffold surfaces of the small and large pore size scaffolds, where small pore size scaffolds had a higer scaffold surface (figure 5.3 B). This then also resulted in a very significantly higher difference in scaffold surface to volume ratio for small pore size scaffolds compared to large ones (figure 5.3 D). The wall thickness of the SF structure was measured to be significantly thicker in large pore size scaffolds (figure 5.3 E), whereas there was a very significantly lower wall number in large pore size scaffolds (figure 5.3 F). The structure model index, describing the plate-rod characteristics of the walls showed that both scaffold types had wall shapes somewhere between plate and rod shape, although the wall of small pore scaffolds were more rod-like (figure 5.3 G). The concectivity density showed also extremly significant differences between small and large pore size scaffolds (figure 5.3 H).

The porosity of SF scaffolds was calculated from the value scaffold volume density (BV/TV, [%]) representing the silk volume per total volume. The porosity [%] of the scaffolds is equal to 100-(BV/TV). In table 5.1 the porosity of 4 scaffolds for small and large pore sizes were listed and the average porosity per pore size was calculated.

With an average of 86.0±0.8 % and 87.1±0.7 % porosity for small and large scaffold pore sizes, no significant difference using an unpaired t-test could be found.

As already seen in the SEM and microCT images the pore sizes within one scaffold varied. The evaluation and analysis of microCT measurements allowed the accessment of pore size distribution within one scaffold. Therefore bins of 6 μm pore diameter

were made and pores found within this pore size range were counted. The distributions were averaged over 4 scaffolds of the same pore size and were fitted with a gaussian distribution, shown in figure 5.4. The mean pore size with standard deviation (SD) for small pores was calculated to be 75.1±28.6 μm and for large pores 116.5±47.5 μm from the gaussian distribution.

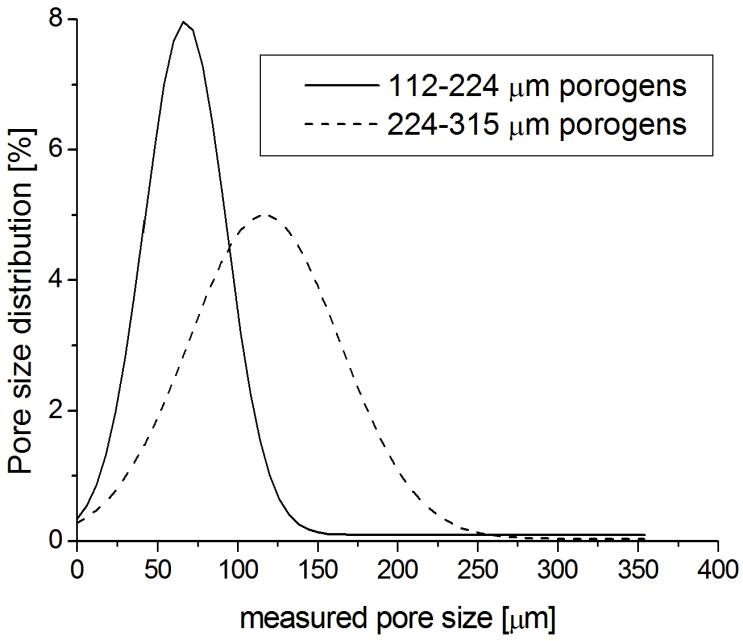

Figure 5.4: Pore size distribution in SF scaffolds made from 112-224 μm or 224-315 μm NaCl porogens. The distributions represent an average of 4 scaffolds (n=4), which were fitted by a gaussian distribution.

Comparing the calculated mean pore sizes found in the scaffolds to the porogen sizes used for scaffols production, it is seen, that for small pore size scaffolds the mean pore size is only 33.5-67.1% of the porogen diameter, whereas for large pore size scaffolds the mean pores are around 37.0-52.0% of the NaCl porogen size.

5.2 Discussion

SEM images (figure 5.1) showed, that SF scaffolds produced from smaller NaCl porogens resulted in scaffolds with smaller pores compared to scaffolds produced with larger NaCl crystals. The SEM images also demonstrated, that within one scaffold, different pore sizes can be seen. For small pore scaffolds NaCl crystals with diameter between 112-224 μm and for larger pores NaCl porogens in the range of 224-315 μm in diameter

have been used for production, this explained on one hand why within one scaffold there were found a range of different pore sizes. Another reason why on SEM images different pore sizes were seen, is that a topographic top view image showed also pores which were not cut in the pore center, seeming to have a smaller diameter than it actually would have. An additional point, which had to be considered is, that SEM images showed just a cut-out of the whole scaffold top surface. The wall thickness and also the wall structure, which seemed to be rather smooth with just a few deepenings, was on all the scaffolds of both pore sizes similar, showing that the actual production process induced no material differences.

To compare the actual structural differences of whole scaffolds it was easier to consider microCT images and the calculated morphometric indices than just sections of top view images by SEM. MicroCT images of the silk fibroin structure (figure 5.2) disclosed similar wall thickness within scaffolds, with just a few bigger trabecular structures. The pore sizes seen in the void volume images (figure 5.2 right column) unraveled non uniform pore sizes within the scaffolds, which was already seen in the SEM images. Although overall the pore sizes of smaller pore scaffolds were smaller compared to larger pore scaffolds. Between SF batches no obvious differences were found.

MicroCT analysis provided morphometric indices which could be easily compared. Scaffold volume was seen to be not significantly different between scaffold types. Which then implies, that there is also no difference in scaffold volume density. The significant difference in scaffold surface (figure 5.3 B) can be understood with considering that in this scaffolds the SF walls were thinner, but more of them in the same volume. So, if the same SF volume is distributed on more SF wall a higer scaffold surface will be created. This then implies directly also a higher scaffold surface to volume ratio for small pore size scaffolds. All this morphometric indices can be compared to a similar study where even more scaffold types with also smaller and larger pores were characterized [54]. All morphometric indices were in a similar range although through higher differences compared to other scaffold types the values had no significant differences between the same pore sizes, which were investigated in this study. The porosity which is calculated from the scaffold volume density also shows no difference between pore sizes. The porosity of scaffolds with different pore sizes stays relatively constant, as previously shown [54]. Although there have been found values around 88% porosity compared to our found results of 86-87.1% porosity, which are a bit lower but still in a comparable range.

MicroCT data also confirm, that there is a pore size distribution within scaffolds. Figure 5.4 shows clear, that pores found in the scaffolds have sizes which are normally distributed. The mean pore sizes measured by microCT compared to porogen sizes

showed a pore shrinkage. This shrinkage is quite huge and one explanation would be, that NaCl porogens could shrink already during processing, having smaller porogens in the actual scaffolds. Although the major reason for this shrinkage would be, that microCT measurments have been done on dry SF scaffolds, which already seen by eye shrink during drying. As the SF scaffolds were produced in a wet state but imaged with SEM and microCT in a dry state also the pore sizes were decreasing during the drying process. What should be always considered is, that the SF scaffolds were produced by hand and could therefore be optimized concerning homogeneity.

Taken together, no clear differences comparing scaffolds of the same pore size from different SF batches could be found, but there are siginificant differences between smaller and larger pore size scaffolds.

Chapter 6

2D culture of MC3T3 osteoblasts

A culture of MC3T3 osteoblasts in 2D was conducted to compare different cell seeding densities and two different osteogenic media with the aim to unravel the best culturing conditions for this osteoblast-like cell line. Two repeated experiments were done where low passage numbers of MC3T3 osteoblasts were seeded at densities of 1.2, 2.4 or 5.2x10^4 cells/well in 24-well plates and cultured in 6 different media for 16 and 26 days or 18 and 28 days. As culturing media maintenance media (1), partially osteogenic media (2, 4, 5) and osteogenic media (3, 6), which contained osteogenic factors ascorbic acid (AA) and β-glycerophosphate (β-G) were used (4.3.4). After culturing period collagen production and mineralization were determined and quantified using Sirius Red and Alizarin Red (ARS) assays, respectively. DNA quantification and Alkaline Phosphatase (ALP) activity to unravel the amount of cells in the culture and their differentation state were determined on day 26.

6.1 Results

6.1.1 Quantification of DNA content

DNA quantification was done on cells cultured for 26 days. The assay does quantitatively detect dsDNA in the presence of ssDNA, RNA or free nucleotides, therefore the quantified DNA is a measure for the amount of cells in the culture. Diagrams listing the quantified DNA per cell concentration and different media of all conditions are shown in image 6.1.

Statistical analysis using one-way ANOVA for repeated measurements were done comparing the different media within the same cell seeding density, where just in the lowest seeding denstiy statistical significant differences between media 1 and 6 as well as 3 and 6 were found (figure 6.1). Comparing the values between the different seeding

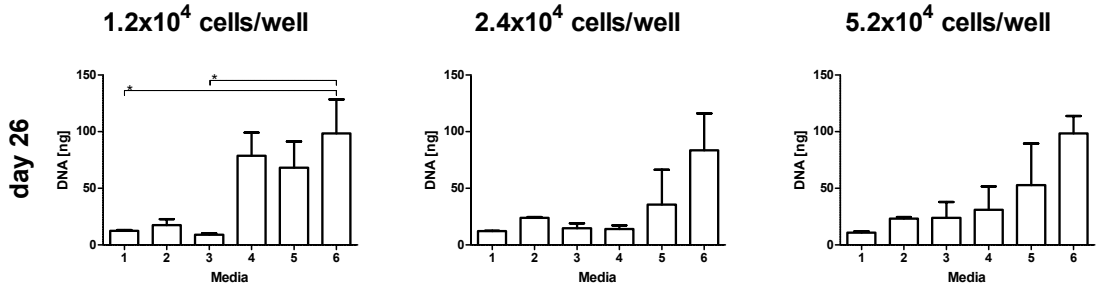

Figure 6.1: DNA quantification representing number of MC3T3 osteoblasts cultured for 26 days at cell concentrations of 1.2, 2.4 or 5.2x10^4 cells/well in 24-well plates in 6 different media (1-6). Values represent mean values of 3 replicates with SEM shown as error bars. Statistical differences are analyzed by one-way ANOVA for repeated measurements, where a p-value < 0.05 (*) represents statistically significant, $p < 0.01$ (**) very significant and $p < 0.001$ (***) extremly significant differences.

densities showed no big differences in DNA content measured at day 26 (figure 6.1). One-way ANOVA statistical analysis of the same media comparing different cell seeding densities revealed also no significant differences (data not shown). DNA content was used as a measure for cell proliferation, as the same cell number were seeded per media in the same cell seeding density group. In media 4, 5 and 6 higher DNA contents were found at day 26 in all seeding densities compared to the maintenance media 1 or media 2 and 3 (figure 6.1).

6.1.2 Quantification of Alkaline phosphatase (ALP) activity

Alkaline Phosphatase is a hydrolase enzyme which catalyzes dephosphorilation. Osteoblasts express a bone specific isoform of ALP and therefore the ALP activity is used as an osteoblast differentiation marker. In figure 6.2 diagrams showing the amount of product (p-nitrophenol), converted by the enzyme ALP from the starting material p-nitrophenylphosphate, normalized per DNA of three different cell concentrations and 6 different media at day 26.

ALP activity measurements of MC3T3 osteoblasts showed, that again between the different cell seeding densities for each media there was no significant differences found by one-way ANOVA statistical analysis (data not shown). Media 1 to 6 within the same cell seeding densities were seen, that maintenance media 1 and also media 2 and 3 had higher ALP activity than media 4, 5 and 6 (figure 6.2). Comparing just the two osteogenic media 3 and 6, it was seen, that MC3T3 osteoblasts expressed 5 to 10 times higher ALP activity in osteogenic media 3 than in media 6 for all cell

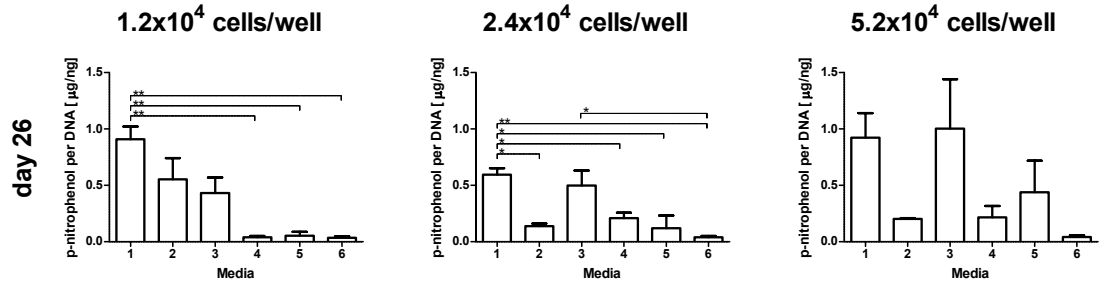

Figure 6.2: Alkaline phosphatase activity quantification of MC3T3 osteoblasts cultured for 26 days at cell concentrations of 1.2, 2.4 or 5.2x10^4 cells/well in 24 well-plates in 6 different media (1-6). Values represent mean values of 3 replicates with SEM shown as error bars. Statistical differences are analyzed by one-way ANOVA for repeated measurements, where a p-value < 0.05 (*) represents statistically significant, $p < 0.01$ (**) very significant and $p < 0.001$ (***) extremly significant differences.

seeding densities, although this difference was just in the middle cell seeding density statistically significant (figure 6.2).

6.1.3 Sirius Red staining and quantification

MC3T3 osteoblasts cultured for 26 days were stained with Sirius Red, as this dye intercalates within collagen fibers and therefore can be used to analyze collagen production of cultured osteoblasts. Images of Sirius Red stained cells cultured for 26 days in wells were shown in figure 6.3.

It is rather difficult to distinguish between positive and negative staining in the wells. But it seems, that in maintenance media 1 no collagen were produced by the cells, whereas in all other media more or less red staining can be seen (figure 6.3). In some wells the cell sheets were clumped together (e.g. figure 6.3 media 3 highest cell seeding density) or cell clots were even lost during media exchange. The most intense staining was found on the edges of the cell sheets, where the cells were rolled up and therefore more condensed (figure 6.3).

To analyze the staining patterns of Sirius Red stained MC3T3 osteoblasts bright field light microscopy images of the stained cells were taken. Images of Sirius Red stained cell sheets cultured for 26 or 28 days at three different cell concentrations in the two investigated osteogenic media 3 and 6 were presented in figure 6.4.

Sirius Red stainings of cells cultured in osteogenic media 3 and 6 showed similar staining patterns for day 26 and 28 for the same media (figure 6.4). Cells cultured in media 3 showed Sirius Red staining which was more distinct along the sides of the cells

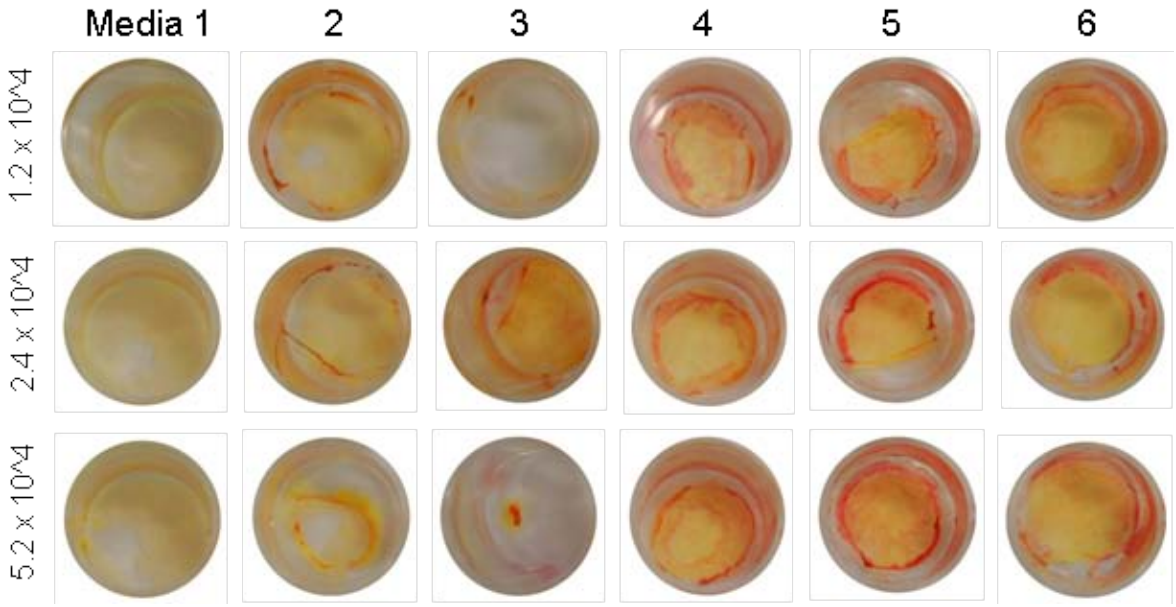

Figure 6.3: Images of Sirius Red stained MC3T3 osteoblasts at three different cell concentrations (1.2, 2.4 or 5.2x10^4 cells/well) at day 26 grown in 24-well plates in 6 different media (1-6).

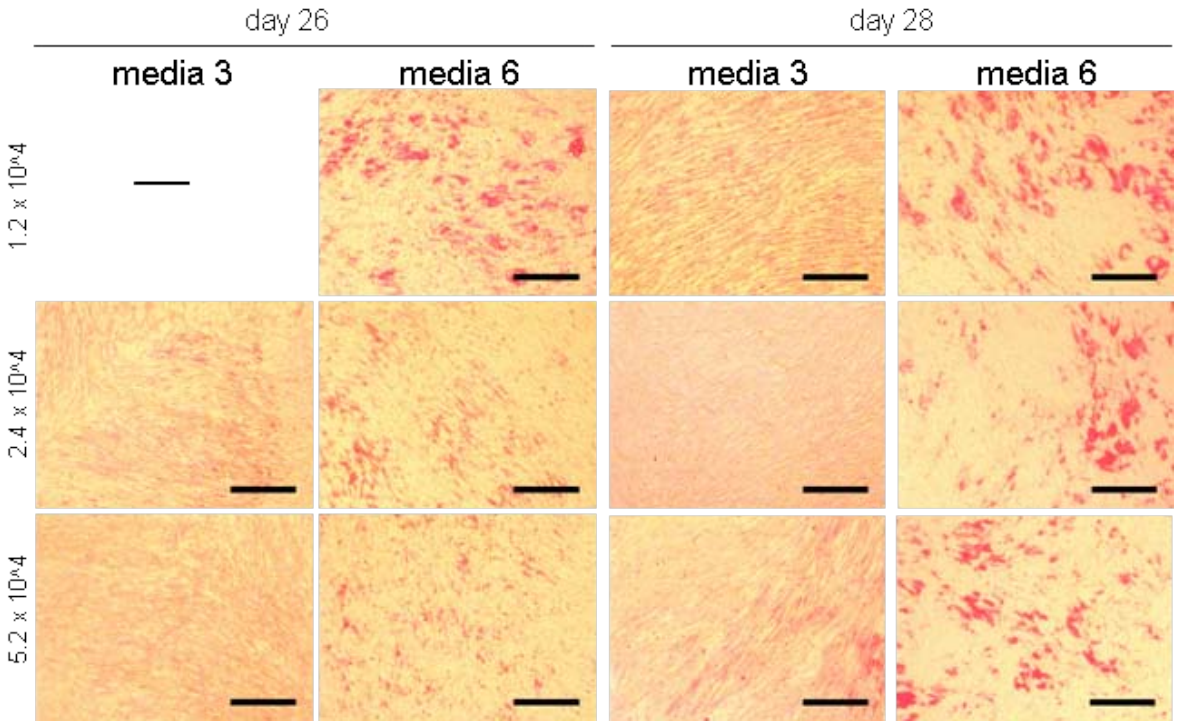

Figure 6.4: Bright field microscopy images of Sirius Red stained MC3T3 osteoblasts seeded at three different cell concentrations (1.2, 2.4 or 5.2x10^4 cells/well) in 24 well-plates and grown in two different osteogenic media 3 and 6 for either 26 or 28 days. The scale bars in the images represent a length of 200 μm.

and more spread all over the cell sheet for all seeding densities (figure 6.4). Whereas cells cultured in osteogenic media 6 showed for all cell seeding densities a different staining pattern compared to media 3. In media 6 the red staining was observed mostly in aggregates on distinct spots, although the staining had a higher intensity (figure 6.4).

Sirius Red stainings on MC3T3 osteoblasts were quantified colorimetrically after disolving the dye in an acidic solution. The measured absorbances for cells seeded with 3 different density cultured in 6 different media for either 16 or 26 days were shown in figure 6.5.

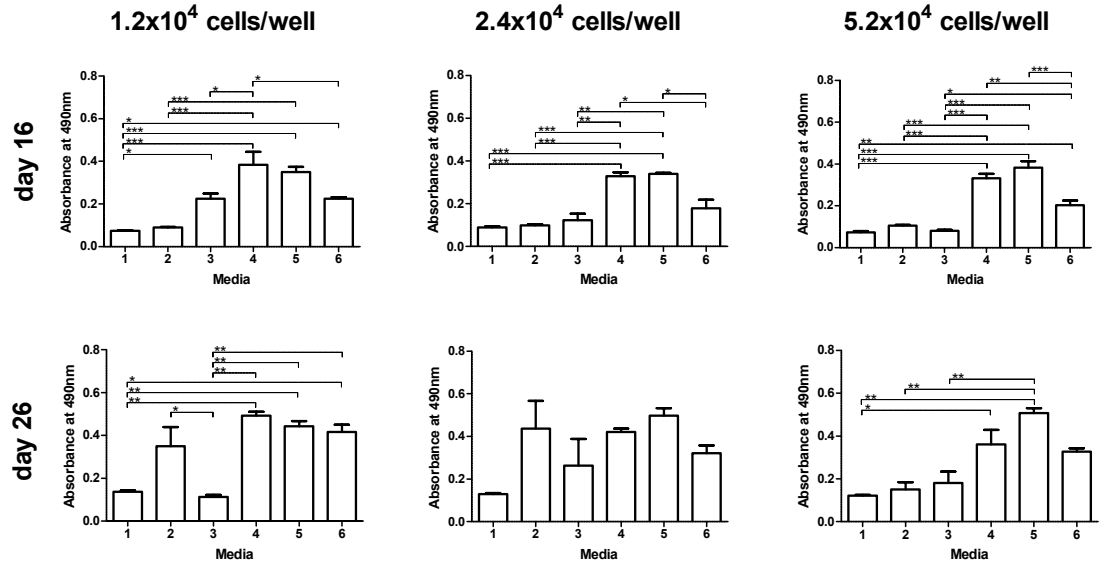

Figure 6.5: Sirius Red quantification representing amount of collagen produced by MC3T3 osteoblasts when cultured for 16 or 26 days at cell seeding densities of 1.2, 2.4 or 5.2x10^4 cells/well in 24-well plates in 6 different media (1-6). Values represent mean values of 3 replicates with SEM shown as error bars. Statistical differences are analyzed by one-way ANOVA for repeated measurements, where a p-value < 0.05 (*) represents statistically significant, $p < 0.01$ (**) very significant and $p < 0.001$ (***) extremly significant differences. Results are representive for two separate experiments.

Sirius Red quantification at an first time in culture at day 16 showed, that in all three seeding densities the highest absorbance was measured in media 4, 5 and 6, whereas the lowest absorbance was detected for cells cultured in maintenance media 1 and a bit higher absorbances were found for cells cultured in media 2 and 3 (figure 6.5). Statistically significant differences were found, but when comparing the two osteogenic media 3 and 6 a significant higher absorbance in media 6 was found just at a middle cell seeding density (figure 6.5). At a later time in culture at day 26, the highest

absorbance for Sirius Red quantification was still found for cells cultured in media 4, 5 and 6. Overall for all conditions an increase in absorbance compared to day 16 of culture was seen (figure 6.5). Though, absorbance measured for cells in media 2 and 3 had the largest increase in absorbance from day 16 to day 26 (figure 6.5). The results are representative for two seperate experiements, as in MC3T3 osteoblasts culture for 18 and 28 days similar quantifiacations for Sirius Red stainings were measured (data not shown).

6.1.4 Alizarin Red staining and quantification

MC3T3 osteoblasts were cultured for 26 days in 24-well plates, fixed with PFA and stained for Alizarin Red (ARS). ARS is a dye, which binds to calcium deposits of mineralization found in the mineralized extracellular matrix produced by osteoblasts. ARS is therefore used as a staining for mineralization. Images of ARS stained cells in 24-well plates cultured for 26 days in 6 different media (1-6) at three different cell seeding densities are presented in figure 6.6.

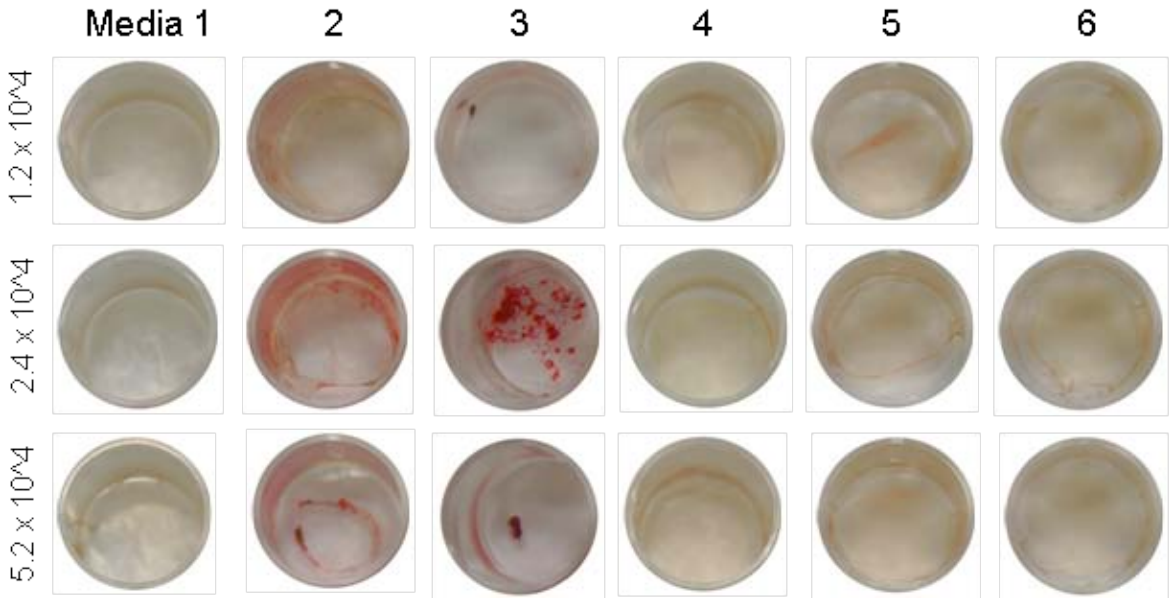

Figure 6.6: Images of Alizarin Red stained MC3T3 osteoblasts at three different cell seeding densities (1.2, 2.4 or 5.2x10^4 cells/well) in 24-well plates at day 26 cultured in 6 different media (1-6).

Alizarin Red staining has been done on the same osteoblasts before Sirius Red staining. ARS staining on osteoblasts in wells was found to be positive for cells cultured in media 2 and 3, whereas at day 26 no staining was found in media 1, 3, 4 and 6 (figure 6.6). The cell sheets were sometimes clumped together or even lost during

media exchange. Cell clumping was most often found on cells cultured in media 2 or 3.

To study the staining pattern and mineralization nodules within the extracellular matrix produced by MC3T3 osteoblasts, bright field microscopy images of ARS stained cells were taken. ARS staining pattern seen on BF microscopy images for cells cultured in osteogenic media 3 and 6 at three different cell seeding densities at day 26 or day 28 are depicted in figure 6.7.

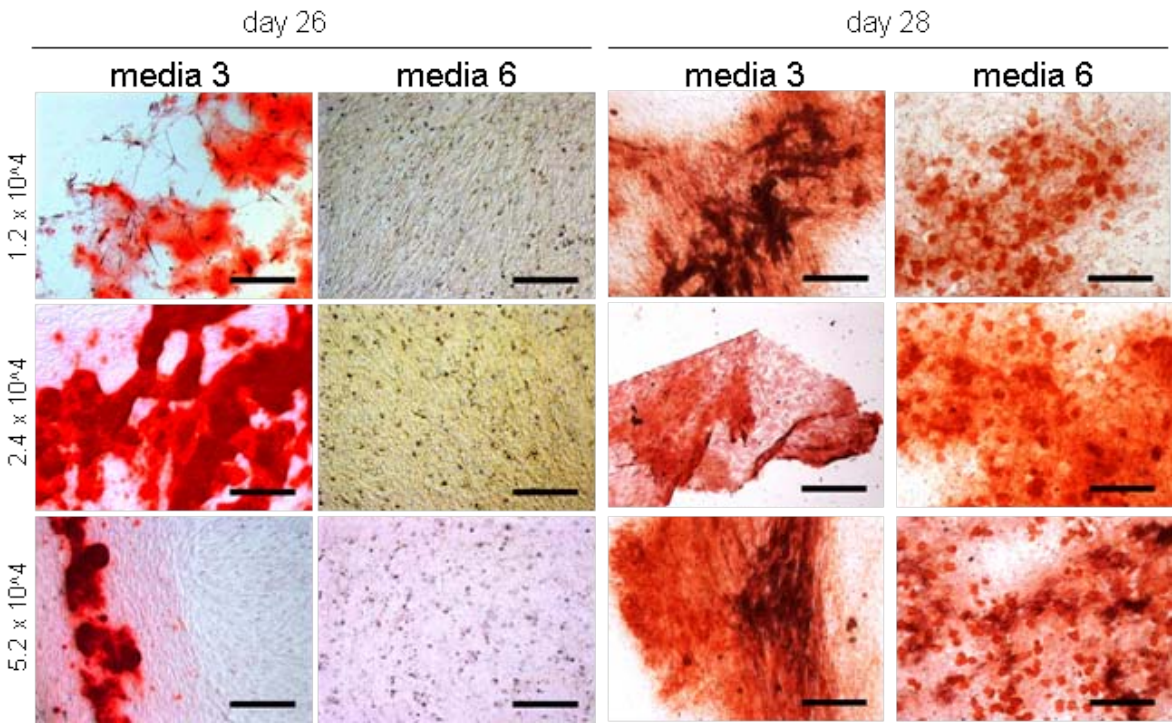

Figure 6.7: Bright field microscopy images of Alizarin Red stained cells at three different cell seeding densities (1.2, 2.4 or 5.2x10^4 cells/well) in 24-well plates cultured in two differenct osteogenic media 3 and 6 for either 26 or 28 days. The scale bars in the images represent a length of 200 μm.

The MC3T3 osteoblasts, which were cultured for 26 days, showed positive staining for all cells cultured in osteogenic media 3, whereas no staining for ARS was seen in cells cultured in osteogenic media 6 (figure 6.7). In the lowest cell seeding density in media 3 (day 26) there were a lot of cells lost during media change, the left cells still were positively stained for ARS. The staining pattern for cells in media 3 was seen to have stained dense mineralization nodules within the cell layer (figure 6.7). Images made from cells cultured for 28 days had not only in media 3 but also in media 6 positive staining for Alizarin Red. The staining pattern for cells in media 3 showed again dense mineralization nodules with even crystaline structures in the strongest stained regions

(figure 6.7). In media 6 the staining was not showing minerlaization nodules, but rather mineralization dots spread over the cells sheet with less strong stained regions for all cell seeding densities (figure 6.7).

The ARS staining was similar to Sirius Red staining disolved with an acidic solution and colorimetrical quantification was done. The measured absorbances of the solutions from cells cultured for 16, 26 and 28 days in all 6 media and three cell seeding densities were presented in figure 6.8.

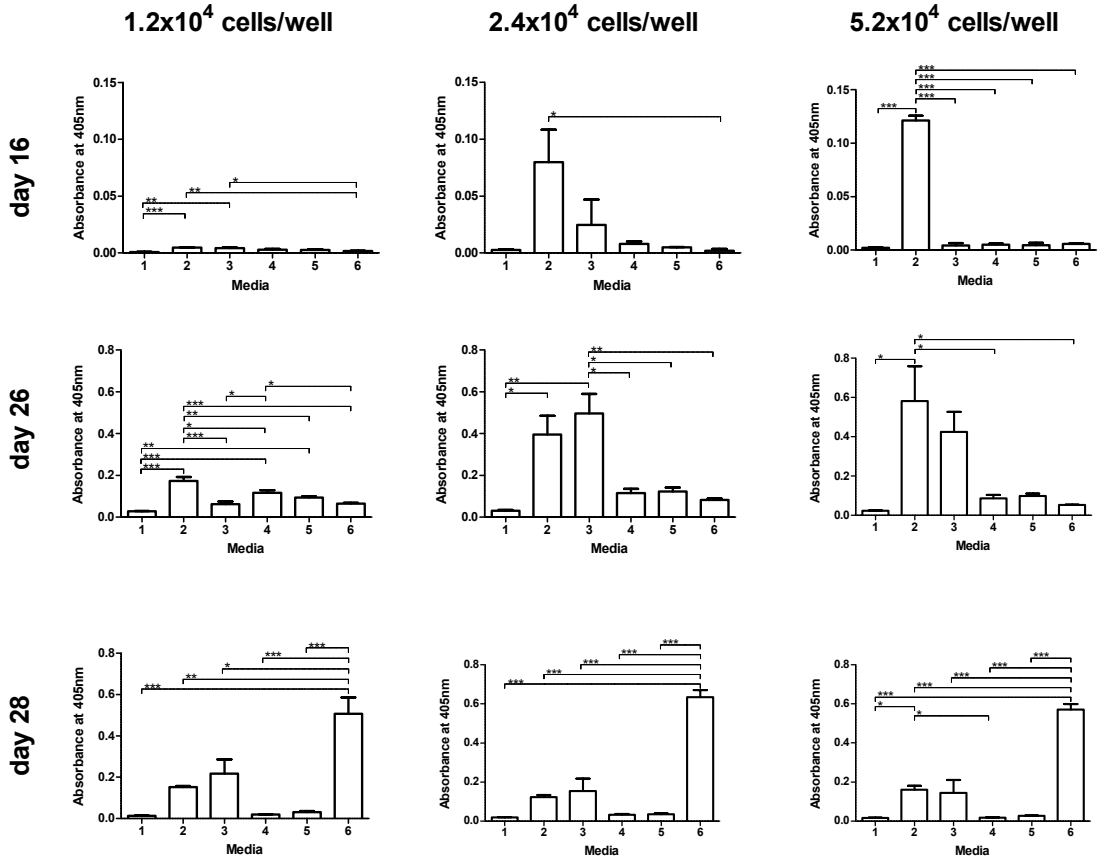

Figure 6.8: Alizarin Red quantification representing amount of calcification by MC3T3 osteoblasts cultured for 16, 26 or 28 days at cell seeding densities of 1.2, 2.4 or 5.2x10^4 cells/well in 24-well plates in 6 different media (1-6). Values represent mean values of 3 replicates with SEM shown as error bars. Statistical differences are analyzed by one-way ANOVA for repeated measurements, where a p-value < 0.05 (*) represents statistically significant, $p < 0.01$ (**) very significant and $p < 0.001$ (***) extremly significant differences.

Alizarin Red quantification showed to be very low in all media besides media 3 and 4 at day 16 (figure 6.8). Similar results have been measured at day 18 (data not shown), although there all media had relatively low absorbances below 0.03. At a later

time in culture, at day 26 the cells were measured to have more mineralization in all media compared to day 16, where the highest absorbances were measured in media 2 and 3 (figure 6.8). In a separate experiment MC3T3 osteoblasts were cultured for 28 days. There absorbances of Alizarin Red were quantified to be low in media 1, 4 and 5 and higher in media 2, 3 and 6 (figure 6.8).

6.2 Discussion

The DNA assay at day 26 showed, that osteoblasts in media 1, 2 and 3 were less proliferating as osteoblasts in media 4, 5 and 6 (figure 6.1), as the same amount have been seeded at the start of the culture. Comparing the DNA content with the ALP activity measured at day 26, the trend is opposite, so that osteoblast, which did not proliferate much according to the DNA content had the highest ALP activity. ALP activity is used as a marker for the osteoblast differentiation lineage. Thus, cells differentiated in the direction of osteoblasts should start to express ALP [47]. The diagrams were normalized per ng DNA, as the ALP activity should be normalized to the amount of cells present. ALP activity compared to DNA content demonstrated, that cells are either proliferating or differentiating. It is therefore surprising, that the ALP activity of osteoblasts cultured in maintenance media 1, which should not stimulate differentiation had such a high ALP activity. Although one needs to consider, that ALP activity is known to rise for cells differentiated into osteoblasts, but the activity is not permanent high [47]. Comparing the two osteogenic media 3 and 6, media 3 showed to differentiate the osteoblasts more than media 6, where they rather proliferated (figures 6.1 and 6.2). Comparing the three different cell seeding densities, there were no significant differences found for all the 6 media, indicating that already the lowest cell seeding density contained enough cells (figures 6.1 and 6.2).

After cells are differentiated into osteoblasts, the cells should start to secrete extracellular matrix, which consists mostly of collagen fibers. Then in a later physiologic stage, osteoblasts should start to deposit mineralization within the ECM [26]. Therefore first collagen fibers should be detected by Sirius Red and then also mineralization nodules should be visible, which can be stained with Alizarin Red. There was the problem of cell sheets which clumped together and formed cell clots. This happend more often the longer the cells were cultured and may indicate, that the cells rather prefered a three-dimensional environment, than to be in a layer. Sirius Red and Alizarin Red stainings and especially quantification on clotted cells were probably no more accurate, as the dye needed to penetrate in and out of the cell clot, which might needed more

time due to longer diffusion distances.

Sirius Red quantification showed collagen production in both osteogenic media. Although in media 6 there was a higher absorbance measured, the difference between media 3 and 6 were mostly not significantly different (figure 6.5). Still, the two osteogenic media showed different Sirius Red staining patterns (figure 6.4). The pattern for media 3 was seen to be more disperse all over the cells, which might indicate a better distributed ECM for further bone-like tissue formation than the more aggregated staining pattern found for media 6 (figure 6.4).

Alizarin Red quantification showed again for both osteogenic media mineralization although media 6 had just in the experiment over 28 days substantial mineralization produced (figures 6.7 and 6.8). Taking into account, that day 16 and 26 experiments were conducted simultaneously with the same passage number and also day 18 and 28 experiments, it seems that cells used in day 18/28 experiments were differentiating slower than cells used in day 16/26 experiments. Taken together, at day 16 or 18 the full mineralization potential was not yet exploited. MC3T3 osteoblasts according to these experiments seem to need around 26 to 28 days to produce nice mineralization nodules. Also the Alizarin Red staining revealed different staining patterns for the two osteogenic media 3 and 6. Comparing the staining patterns to mineralization nodules formed from embryonic stem cells, neonatal calvarial osteoblasts and mesenchymal stem cells also cultured for 28 days, the pattern seen with media 3 seems to be more physiological [17].

As already found in DNA and ALP activity assays, the cell seeding densities were also in Sirius Red and Alizarin Red staining and quantfication not causing any real differences. Any statistical differences seen in the Sirius Red and Alizarin Red quantification between cell seeding densities should always be treated carefully, as especially in media 2 and 3 often cells were lost during media exchange, which then may dramatically reduce the actual collagen production as well as mineralization in the condition. The actual used cell seeding densities are in the same range as has been used previously [37].

Finally, osteogenic media 3 (BGJb with AA and β-G) was seen to be the better osteogenic media for MC3T3 osteoblasts based on the mineralization nodule structure, the collagen distribution seen by Sirius Red staining and the higher ALP activity, indicating differentiation to osteoblasts, in comparison to osteogenic media 6 (MEM alpha with AA and β-G). The cell seeding densities were showed to have no big effect on the differentiation, collagen production and ECM mineralization, therefore the lowest cell seeding density seems to be sufficient for MC3T3 osteoblasts.

Chapter 7

Bone formation on 3D silk fibroin scaffolds in static bioreactors

The experiment aimed to investigate the difference of MC3T3 osteoblast bone formation on SF scaffolds with small and large pore sizes made from NaCl porogens with either 112-224 μm or 224-315 μm diameter. Additionally to the different pore sizes the SF scaffolds were produced from three different silk fibroin batches, which were investigated for bone formation differences. MC3T3 osteoblasts were seeded on the SF scaffolds and cultured for 33 days in static bioreactors in osteogenic media. As osteogenic media the more promising media showin in 2D investigations, BGJb with ascorbic acid and β-glycerophosphate (media 3), was chosen. The cell seeding density on the SF scaffolds was upscaled from the lowest cell seeding density used in 2D investigations. To monitor mineralization during culture, non-destructive microCT imaging was done at day 13, 20, 27 and 33 of culture. Distribution of the mineralization within the scaffolds was visualized by 3D images of the microCT data. After cell culture on some scaffolds biochemical assays were performed to measure DNA concentration and calcium concentration on the constructs. Furthermore Sirius Red and Alizarin Red staining and quantification was done on the SF scaffolds. As well as SF scaffolds with seeded cells, which were cultured for 33 days were fixed and prepared for scanning electron microscopy to analyze the topography of the cell-scaffold constructs. To investigate the distribution of cells, collagen and mineralization within the constructs, SF scaffolds were embedded in paraffin, sectioned and histologically stained for Hematoxylin & Eosin, Sirius Red, Alizarin Red, and von Kossa.

7.1 Results

7.1.1 Biochemical analysis

After culture of MC3T3 osteoblasts on SF scaffolds in static bioreactors for 33 days some of the scaffolds were broken up to analyze DNA content and calcium concentration in the scaffold. As the assays needed to destroy the scaffolds measurements have been done on just one (DNA assay) or two (calcium assay) scaffolds per group. Also Sirius Red and Alizarin Red staining and quantification were done on the scaffolds after culture. Values measured in DNA assay showing the amount of cells in the scaffolds, calcium assay quantifing osteoblast mineralization within the scaffold, Sirius Red quantification representing the amount of collagen produced and Alizarin Red quantification also showing the amount of osteoblast mineralization were shown for SF batches 1 and 2 of both scaffold pore sizes in figure 7.1. All values were normalized to the scaffold wet weight measured after culture to compensate for uneven scaffold volumes.

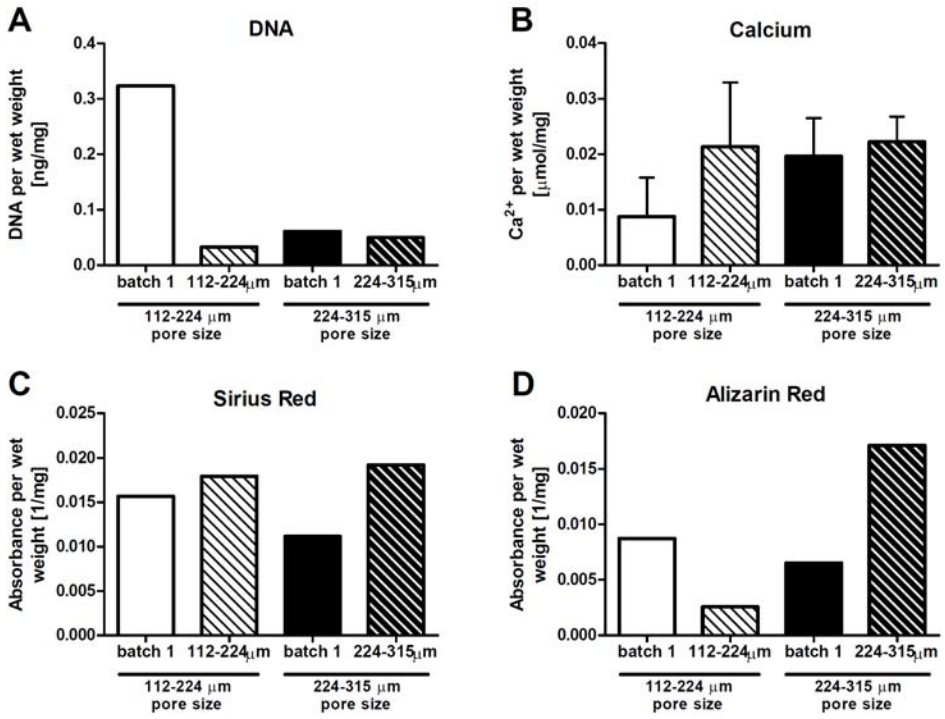

Figure 7.1: DNA (A), Calcium (B), Sirius Red (C) and Alizarin Red (D) quantification of MC3T3 osteoblasts on SF scaffolds made from small (112-224 μm) or large (224-315 μm) porogens and prepared from two different SF batches, which were cultured for 33 days in static bioreactors are shown. Measured values were normalized to the scaffold wet weight measured after culture. The calcium assay (n=2) showed to have no significant differences ($p > 0.05$) between the groups analyzed by one-way ANOVA.

DNA content was seen to be 4 to 8 times higher in the small pore size scaffold from SF batch 1 compared to all other groups, which had below 0.1 ng DNA per mg scaffold wet weight (figure 7.1 A). The calcium assay showed, similar calcium content in large pore size scaffold of both SF batches and also in small pore size scaffolds from batch 2, whereas in scaffolds with small pores made from batch 1 the calcium content was only around half the amount found in the other groups (figure 7.1 B). The Sirius Red assay showed, that in all scaffold groups collagen was produced (figure 7.1 C). Alizarin Red quantification also quantifying minerlization was different for all the scaffold with no clear trend (figure 7.1 D).

7.1.2 MicroCT analysis of osteoblast mineralization during culture

Three-dimensional visualization of microCT data had been done and representative top view images of all scaffold groups at day 13, 20, 27 and 33, as well as cross-sectional view of one scaffold is presented in figure 7.2.

In all scaffolds besides small pore size scaffolds SF batch 1 mineralization was observed already at day 13 (figure 7.2). Mineralization was located sometimes just at the outer edge and started to grow into the middle of the scaffold, or as in small pore size scaffolds SF batch 2 mineralization started on one side of the scaffold and then spread allover the scaffold (figure 7.2). The cross-sectional view showed, that the center of the scaffold was not mineralized at the beginning, which then was filled more and more over culture time (figure 7.2 bottom row).

The mineralization was quantified using the bone volume density calculated from microCT data, which showed the mineralized volume per total volume of the chosen mask. Bone volume density was the only morphometric index, which made sense to use. Bone volume density of MC3T3 osteoblasts cultured on small or large pore sized SF scaffolds from 2 or 3 different SF batches were measured at day 13, 20, 27 and 33 and the values showed in diagrams in figure 7.3. Data could be averaged for scaffolds with same pore size produced from the same SF batch, as statistical analysis with one-way ANOVA showed no significant differences within the groups.

Again, in small pore size scaffolds from batch 1, nearly no mineralization occured over the whole culture time, whereas in all other scaffold groups, the mineralization was increasing over time reaching end values of up to 13% bone volume density (figure 7.3). The only statisically significant differences were found between small pore size scaffold batch 1 and small pore size scaffolds batch 2 as well as between the former one and large pore size scaffolds batches 1 and 2 at all time (figure 7.3). There were

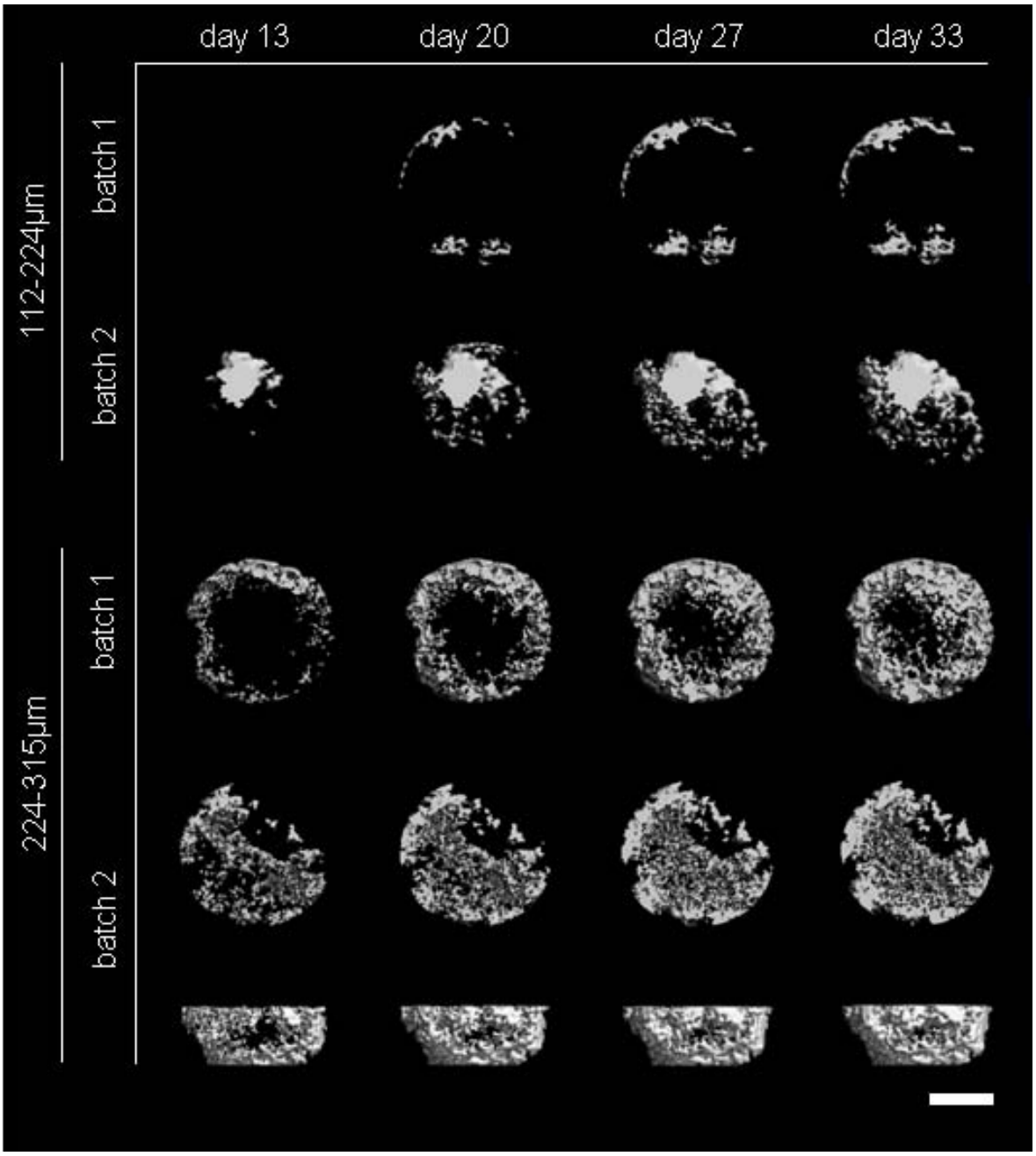

Figure 7.2: MicroCT images showing osteoblast mineralization on SF scaffolds at day 13, 20, 27 and 33 cultured in static bioreactors. The bottom row presents a cross-sectional view of the same scaffold, where as all other images show top views of the scaffolds. The scale bar represents 2mm.

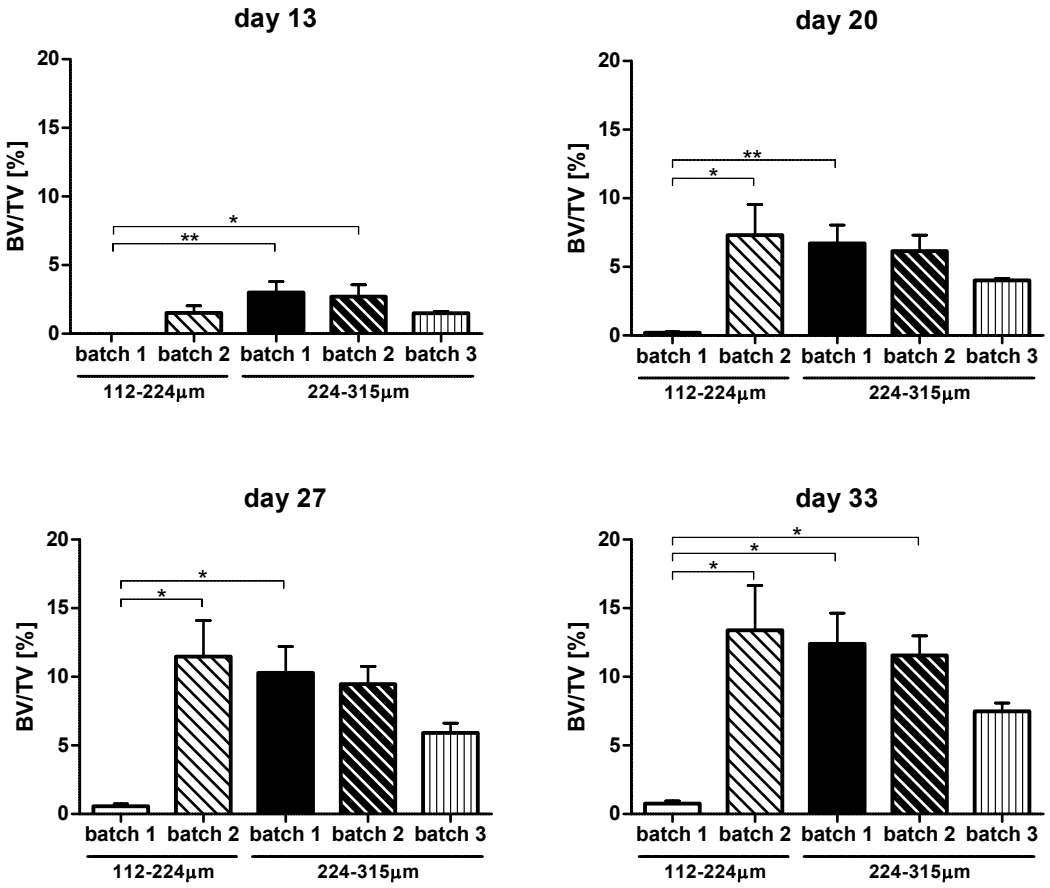

Figure 7.3: Bone volume density (BV/TV) of MC3T3 osteoblasts on SF scaffolds at day 13, 20, 27 and 33 cultured in static bioreactors. SF scaffold with small or large pores made with 112-224 μm or 224-315 μm porogens and produced from 2 or 3 SF batches, respectively. Data is represented as mean $\pm$ SEM of n=6, 5, 6, 6, 2 scaffolds per group. Statistical differences were analyzed by one-way ANOVA (Kruskal-Wallis test with a Dunn's multiple comparison post-hoc), where a p-value < 0.05 (*) represents statistically significant and $p < 0.01$ (**) very significant differences.

no statistically significant differences found between all SF batches of the large pore size scaffolds (figure 7.3). In small pore size scaffolds batch 2 was significantly more mineralized from day 20 on (figure 7.3).

The same data pointing out the increase in mineralization over time on all groups of scaffolds can be seen in figure 7.4.

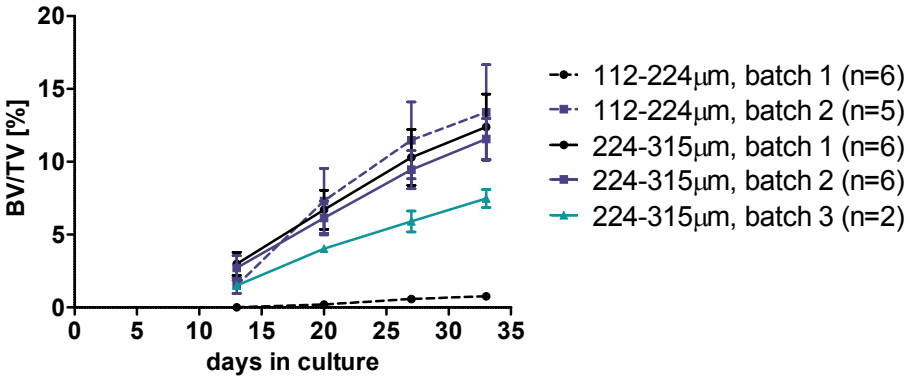

Figure 7.4: Bone volume density (BV/TV) increase over time of MC3T3 osteoblasts seeded on SF scaffolds cultured in static bioreactors are presented. SF scaffolds with small (dashed lines) and large (straight lines) pore sizes produced from different SF batches (1: black, 2: blue, 3: green) were used. Data are presented as mean ± SEM.

Small or large pore size scaffolds produced from SF batch 2 had similar mineralization rates, whereas there was a huge difference between small and large pore size scaffolds from batch 1 (figure 7.4). Although large pore size scaffolds from batch 3 showed slightly slower mineralization, there was no significant difference found between this group and the other large pore size scaffolds (figure 7.4).

7.1.3 Scanning electron microscopy of scaffold-cell constructs

MC3T3 osteoblasts, which were cultured for 33 days on SF scaffold in static bioreactors were fixed and topographic images with SEM were taken. SEM images of cell-scaffold constructs of small pore and large pore size scaffolds produced from SF batches 1 and 2 are depicted in figure 7.5.

Scanning electron microscopic analysis of topography of cell-scaffold constructs revealed on most of the scaffolds cells, although single cells and also extracellular matrix can not be distinguished with this method. No cell was observed on small pore size scaffold form batch 1, but according to the DNA assay this small pore size scaffold from SF batch 1 group should have plenty of cells on the scaffold (figure 7.5 A). On all other scaffolds nice cell layers and net-work like fibers, which connect the cell sheet

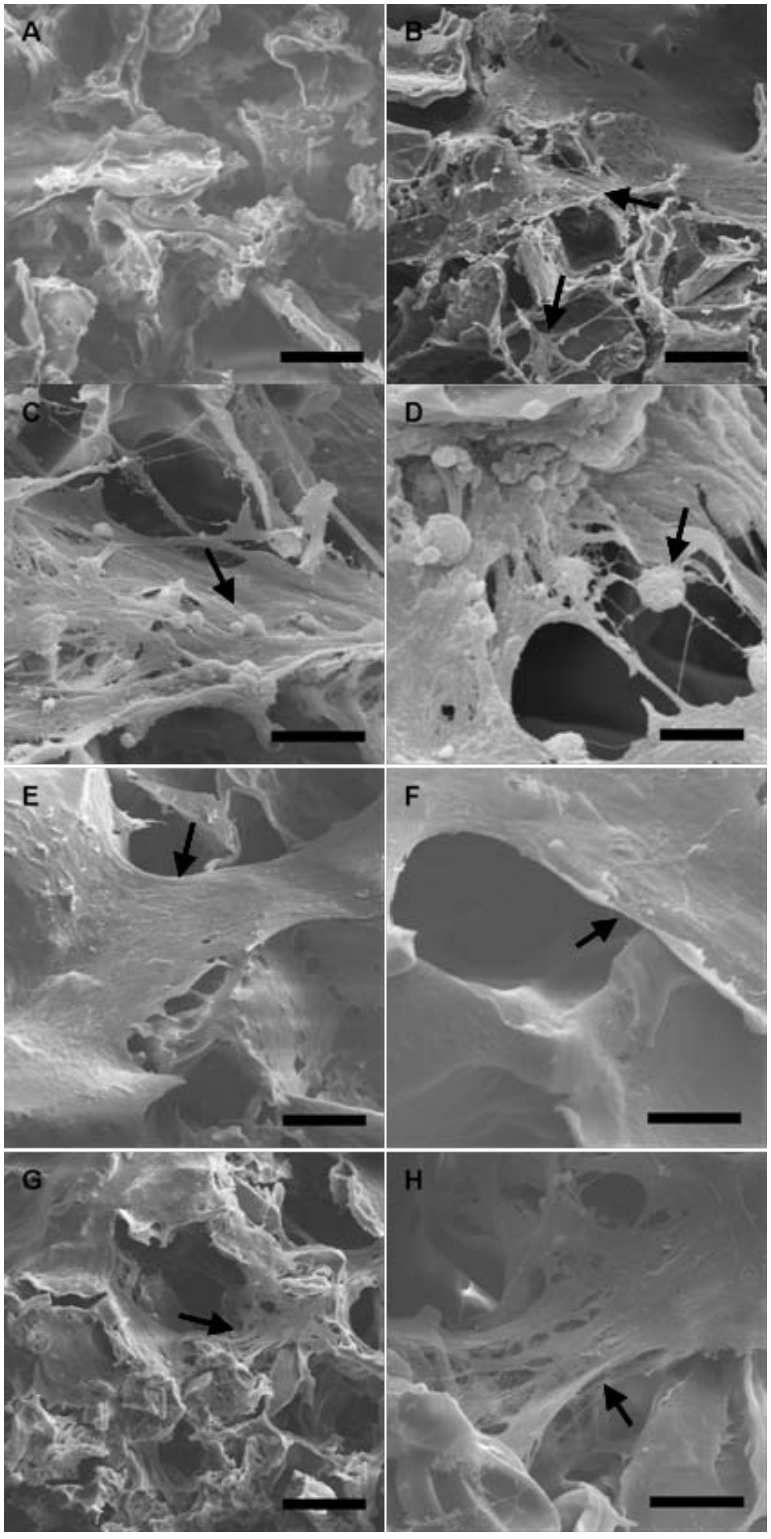

Figure 7.5: SEM images of SF scaffolds with small pore sizes (112-224 μm porogens) (A-D) and large pores (224-315 μm porogens) (E-H) from two different silk batches (1: A, E, F; 2: B-D, G, H) seeded with MC3T3 osteoblasts and cultured for 33 days in static bioreactors. The images show different magnifications; 200x (scale bar 100 μm, A, B, E, G), 900x (scale bar 25 μm, C, F, H) and 2000x (scale bar 10 μm, D). Arrows indicate cells (B, E-H) or mineralization nodules (C, D) found on the scaffolds.

from one side of the scaffold pore to the other were observed (figure 7.5 B-H, arrows). Very interesting are the higher magnification images, as there on fibers and on the cell sheets globule-like structures (see arrows in C and D) were observed (figure 7.5 C and D).

7.1.4 Histology of cell-scaffold constructs

Histological section of MC3T3 osteoblast seeded SF scaffolds have been done after culture. Serial sections were stained for Hematoxylin & Eosin (H&E), Sirius Red, Alizarin Red (ARS) and von Kossa. H&E is a standard histological staining, where on SF scaffolds hematoxylin stains the cell nuclei purple and Eosin stains the ECM as well as the silk fibroin scaffold in a pink color. Sirius Red stains collagen fibers secreted by osteoblasts red, although the SF was sometimes also colored redish. ARS stains calcium deposits of mineralization red and von Kossa staining colors phophate deposits of mineralization dark brown to black. H&E, Sirius Red, Alizarin Red and von Kossa stained sections of small pore size scaffolds produced from SF batches 1 and 2 are depicted in figure 7.6. Sections have been taken of the top and middle part of the scaffolds, where the images were taken at the edge of the scaffolds.

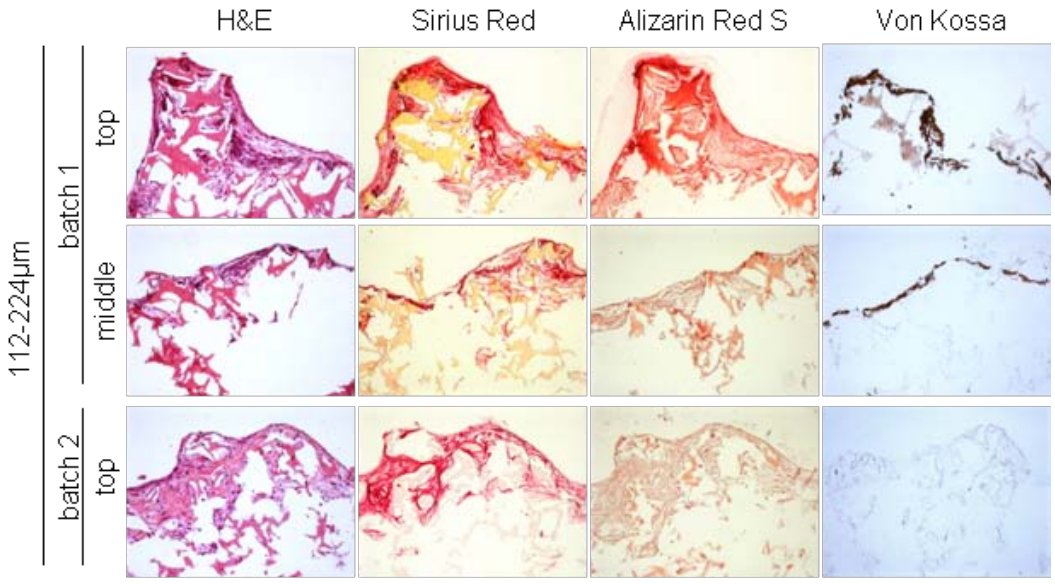

Figure 7.6: Histological sections of paraffin embedded scaffolds seeded with MC3T3 osteoblasts and cultured for 33 days in static bioreactors. Serial sections of 5 μm thickness were stained with Hematoxylin and Eosin, Sirius Red (1mg/ml) for collagen, Alizarin Red (40mM) for calcium deposits and von Kossa (1% silver nitrate) for phosphate deposits. Sections were taken from either the top or the middle part of the scaffold and images were taken at the edge of the scaffold section. All images are taken with a 10x magnification. The scale bar represents a length of 300 μm.

H&E sections of top parts of the scaffold demonstrate many cells within the SF scaffold structure, seen by a lot of positively stained cell nuclei for Hematoxylin. The cells are embedded in ECM in between the scaffold pores and at the outside of the scaffold (figure 7.6). Sirius Red staining on the scaffold sections confirm, that collagen fibers have been produced mostly at the edge of the scaffold (figure 7.6). Alizarin Red and von Kossa stainings show positively stained regions at the edge of the scaffold, indicating mineralized ECM (figure 7.6). Both SF batches show similar cell content, and collagen production, wheras it seems that batch 1 had more mineralized ECM compared to batch 2 (figure 7.6). Comparing top and middle sections there was no trend that just the top or the middle part of the scaffold had more cells, collagen and or mineralization (figure 7.6 and not shown data). Also for large pore size scaffolds histological stainings with H&E, Sirius Red, Alizarin Red and von Kossa have been done on scaffold produced from three different SF batches on top and middle sections of the scaffolds. Images showing scaffold edge or center of histological stained sections are presented in figure 7.7.

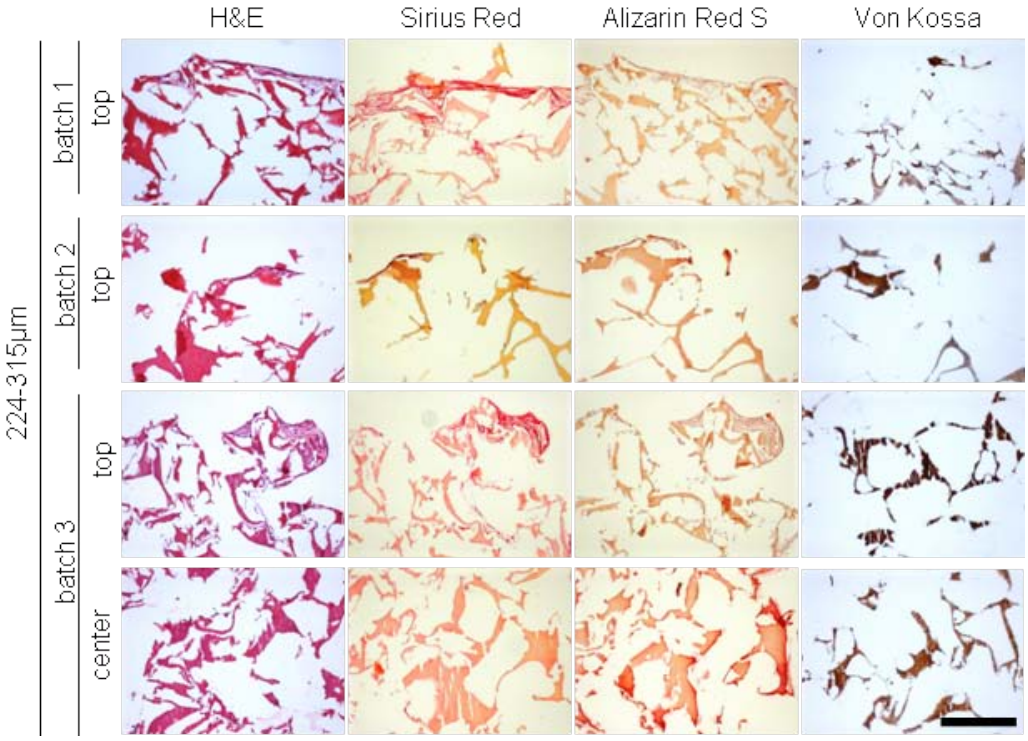

Figure 7.7: Histological sections of paraffin embedded scaffolds seeded with MC3T3 osteoblasts and cultured for 33 days in static bioreactors. 5 μm thick serial sections were stained with Hematoxylin and Eosin, Sirius Red (1mg/ml), Alizarin Red (40mM) and von Kossa (1% silver nitrate). Sections were taken from the top part of the scaffold and images were aquired at the edge or in the center of the section. All images are taken with a 10x magnification. The scale bar represents a length of 300 μm.

Similar cell content, collagen distribution and mineralization have been found in large pore size scaffold sections at the scaffold edge compared to small pore size scaffold sections (figure 7.7). In the center of scaffold sections generally no or few cells were present and hardly no collagen fibers, as well as mineralization was seen (figure 7.7). To better distinguish single structures within the scaffold sections cut-outs of the top sections shown in 7.6 top row are taken and displayed in a higher magnification in figure 7.8.

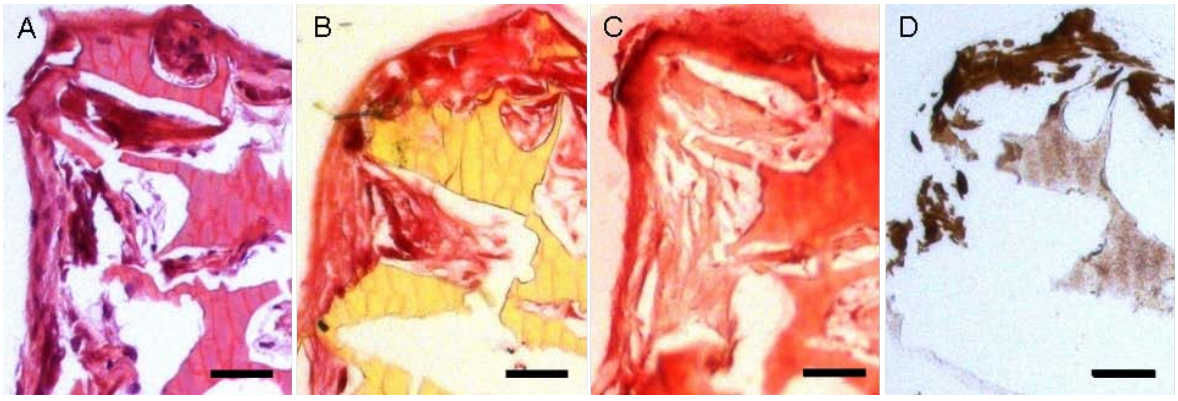

Figure 7.8: Details of serial histological sections of a scaffolds seeded with MC3T3 osteoblasts and cultured for 33 days in static bioreactor. 5 μm thick serial sections of paraffin embedded scaffolds were taken and stained with Hematoxylin and Eosin, Sirius Red (1mg/ml) for collagen, Alizarin Red (40mM) and von Kossa (1% silver nitrate). Images show a detailed cut-out from images shown in the top row of figure 7.6. The scale bar represents a length of 100 μm.

H&E staining showed many cells within scaffold pores and at the scaffold edge. The cells were embedded within dense ECM, which connected the scaffold structures. The SF scaffold itself was stained pink by Eosin and had a striped pattern (figure 7.8 A). Sirius Red staining showed a lot pf positive staining within the ECM surronding the cells, demonstrating that most of the ECM is composed of collagen fibers. The staining allows to distinguish fibrous structures within the ECM. The SF scaffold showed a yellowish background staining (figure 7.8 B). Alizarin Red and von Kossa stained sections showed positive staining on the ECM structure indicating mineralized ECM. Although strong Alizarin staining was seen on the SF scaffold as well as some lighter von Kossa staining (figure 7.8 C and D).

7.2 Discussion

MC3T3 osteoblasts produced extracellular matrix and started to mineralize it also in 3D on SF scaffolds cultured in osteogenic media. The bone volume density calculated

from microCT measurements increased in large and small pore size scaffolds of all SF batches over time. Although, in small pore size scaffolds made from SF batch 1 bone volume density increased significantly slower compared to all other groups. This result could not be explained by a different SF structure, as no differences were found compared to small pore size scaffolds from SF batch 2, which had a similar mineralization rate as large pore size scaffolds. Also large pore size scaffolds made from the same SF batch 1 showed no differences to large pore size scaffolds from batch 2, which indicates, that the deviation was not due to the SF batch 1.

Both mineralization patterns either starting at the outside or from one point were observed in all groups, so there was no evidence, that certain scaffolds mineralize just in a special way. The different starting points of mineralization were probably influenced by the seeding technique of the cells. During cell seeding aliquoted cell suspension containing the needed cell number were added on top of the scaffolds, but it could not be controlled if cells were seeded in the middle of the scaffold top or somewhere rather on the edge. Cross-sectional views of the mineralized scaffolds showed, that especially at the beginning the center of the scaffolds were not mineralized. This leads to the conclusion, that cells may hardly reach the scaffold center or that the center has low nutrient and metabolite exchange due to diffusion restrictions within the scaffold [12]. Nutrient and metabolite exchange within the scaffold could be enhanced by culturing scaffolds in bioreactors, which create a fluid flow through the scaffold by e.g. spinning the media or diffusing the media through the scaffolds [12].

Interestingly, DNA concentration was around 4 to 8 times higher in the small pore size scaffold from batch 1 compared to the other scaffolds. This could be an explanation why hardly no mineralization was observed on small pore size scaffolds of SF batch 1. It seems as if the cells on this scaffolds were just proliferating instead of differentiating and therefore many cells were detected but not a lot of mineralization. The calcium assay which accesses directly calcium ions in the scaffold showed also that small pore size scaffolds from batch 1 had less calcium, respectively mineralization as the other scaffolds. Which would be consistent with the bone volume density measured with microCT. Still, the difference seen in the calcium assay was statistically not significant, but it showed the same trend as the microCT data. Sirius Red assay revealed no big differences between scaffolds, which can be explained as already not so far differentiated osteoblasts start to secrete collagen fibers but do not mineralized the ECM. Assuming, that also cells in small pore size scaffolds from batch 1 were already partially differentiated into the direction of mature osteoblasts, so that they already secreted extracellular matrix. Alizarin Red assay on the other hand should be consistent with the calcium assay, as both quantify mineralization, but Alizarin this was not

the case. One way to explain this, would be that Alizarin Red staining was performed on undestroyed scaffolds, which is more difficult for the dye to penetrate the whole scaffold compared to thin layers. The Alizarin Red data was actually consistent with the fact, that the more destroyed scaffolds showed higher ARS absorbance compared to intact scaffolds. Hence, ARS assay shoule not be considered. In the future ARS assays should be performed on on small cut pieces or even destroyed scaffolds to increase the dye accessibility.

SEM images demonstrated, that cells were present on the cultured SF scaffold and covered pores of the scaffolds with cell layers and ECM. On one scaffold the were no cells observed, although it might be that unfortunately the bottom side of the scaffold was investigated instead of the top, where probably less cells would be present. Still, according to the DNA assay on small pore size scaffolds from batch 1 there should plenty of cells. High magnification SEM images showed glouble-like structures on top of the cell layers and along fibrillar structures. As the theory describes mineralization the way, that first extracellular matrix with collagen fibers are secreted and the collagen fibers then serve as crystallization nuclei, this would indicate, that the observed globules are mineralization nodules on secreted collagen fibers. Similar structures called calcospherulites or nodular accretions were observed in other studies [44, 11].

Scaffold sections showed generally a striated pattern on the scaffold structure, which was likely caused by the blade during sectioning, as the pattern was oriented always in the same direction. Overall, histological sections of scaffold-cell constructs showed that cells, ECM and also mineralization were predominantly found on the outer side of the scaffolds and not in the scaffold centers. Which indicated, that either the scaffold pores were not well interconnected, so that cells were able to migrate into the center or, that inside the scaffold nutrient and metabolite exchange was hindered, so that cells were not able to survive in tha scaffold center. This again should be improved by culturing the cells in e.g perfusion bioreactors, which enhance nutrient and metabolite exchange also in the center of the scaffolds [12].

The cell seeding density used on the scaffolds was upscale from 2D up to the scaffold volume with an assumption of a cell layer thickness of 2.4 μm, as this value was measured for attached MC3T3 cells on Tantalum substrates [2]. Still, one could argue, that the cell concentration calculation did not include the effect of the SF which occupies 13 to 14% of the scaffold volume. But, there was the problem, that it was probably much harder for cells to get into the scaffold and attach tightly compared to just attach on a flat well bottom. Therefore the cell concentration was rather overestimated to get a similar cell concentration on the SF scaffolds after seeding. In other studies

they used MC3T3 osteoblasts on PLGA scaffolds with a 2-3 times lower cell density, although higher passage numbers, which likely proliferate faster have been used [13]. Compared to a study where also MC3T3 on collagen-glycosaminoglycan scaffolds were cultured for 49 hours, we used a 5-6 times higher cell density [25]. Instead, in bone-like tissue engineering with hMSC on SF scaffolds a 6 times higher cell density was used compared to this study [24]. Although MC3T3 cells were used mostly at lower cell densities on other scaffold materials, other osteoprogenitor cells on SF scaffolds were used at a higher density. Allover the used cell seeding density upscale from 2D was chosen accurate, as cells survived during culture and produced mineralized ECM, indicating that bone-like tissue formation was occuring.

To sum up, SF scaffolds were compatible with MC3T3 osteoblasts and support MC3T3 differentiation and minaralisation. It was seen, that significantly less bone volume density was observed in small pore size scaffolds of SF batch 1 compared to all other scaffolds. This might be explained, as according to the DNA assay 3 to 5 times more DNA has been found in this scaffold, which indicates, that cells have been proliferating instead of differentiating as in the other scaffolds. The calcium assay confirms the results of the microCT data, although the trend was not seen in histological sections, which might just be from the fact, that histology concentrated just on some few sections of the whole scaffolds. Histology still showed that cells were present in the scaffolds and that collagen fibers were secreted and partially mineralized, which was also seen in the SEM images of scaffold-cell constructs.

Chapter 8

Mechanical stimulation of osteoblast-like cells co-cultured with macrophages on SF scaffolds

To get tissue engineered constructs into a state where they are competitive alternatives to other auto- or allografts already used clinically the mineralization rate on these constructs needs to be much faster in order to provide a needed graft in a shorter time period. Therefore an alternative physiologic stimuli, elevated extracellular calcium, which could promote faster mineralization was employed. Another stimuli, which can accelerate mineralization rate was seen in mechanical loading of bones. Cylcic loading positively influences bone formation [15] and is therefore expected to induce more mineralization on loaded scaffold-cell constructs compared to non-loaded ones. Thus mechanical stimulation of MC3T3 osteoblasts was applied to unravel the influence of a cyclic sinusoidal stimulation pattern. The setup of the experiment was focused to see differences in control versus high-calcium media and the role of applied loading to osteoblasts in bone tissue engineering. As previously presented, a discrete population of F4/80$^+$ tissue-macrophages (osteomacs) are present *in vivo* forming a canopy structure over bone forming osteoblasts [10]. A depletion of these osteomacs *in vivo* results in a loss of osteoblastic bone forming surface and *in vitro* in a reduction of osteoblast mineralization. Therefore it was proposed that osteomacs stimulate osteoblast differentiation [10]. Thus, the possibility of a co-culturing of RAW 264.7 macrophages with MC3T3 osteoblasts to enhance osteoblast differentiation and mineralization was investigated on SF scaffolds. The experiment was including the stimuli elevated extracellular calcium, cyclic loading and co-culturing of macrophages with osteoblasts. Due to a limited number of bioreactors (12) and the absolute need to include appropriate controls, the experiment was done with one scaffold per treatment.

8.1 Results

The experimental time line included cell seeding, mechanical stimulation every 2-3 days and microCT monitoring every 3-4 days. At day 13 the scaffolds were analyzed for ALP activity and DNA content of one half of each scaffold and the other halves were fixed with PFA and embedded in paraffin for histological analysis. The experimental time line is presented in figure 8.1.

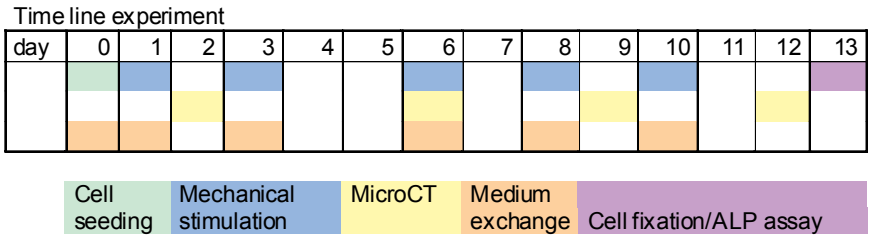

Figure 8.1: The timeline of the co-culture experiment of MC3T3 osteoblasts with RAW 264.7 macrophages is shown including the exact time points of cell seeding, media exchange, microCT scanning, mechanical stimulation and cell fixation during culturing.

8.1.1 Biochemical assays

After 13 days culture time the scaffold-cell constructs were cut in half and one half was used to analyze DNA content and ALP activity. DNA concentration was measured and the values were normalized to the measured scaffold wet weight to compensate for imprecise scaffold cutting or uneven total scaffold weights. The ALP activity was measured on the same samples as the DNA content and therefore represents an overall ALP activity of the cells from this scaffold halves. To compare ALP activity per cell the measured enzyme was normalized to the DNA content of the samples. DNA content and ALP activity of scaffolds seeded with cells and cultured in all treatments are shown in figure 8.2.

The amount of DNA present in the scaffolds represents how many cells there are present and therefore it is a marker of how much the cells proliferated. Whereas the ALP activity quantifies the amount of the enzyme alkaline phosphatase on the cell surface of osteoblastic cells and is used as an osteoblast differentiation marker. On small and large pore size scaffolds there was more DNA content found on scaffolds seeded with just OB compared to scaffolds seeded with OB and MΦ, with generally more DNA in scaffolds cultured in control media (figure 8.2 A, B). There was also

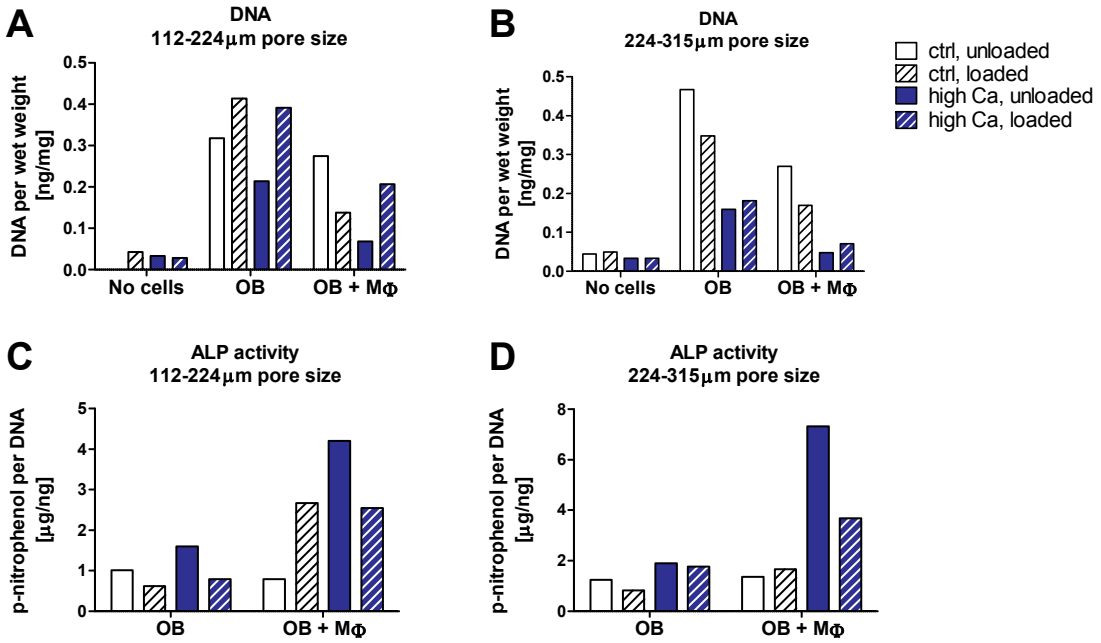

Figure 8.2: ALP activity and DNA concentration on scaffolds cultured in MSU bioreactors with either no cells, MC3T3 osteoblasts (OB) or OB and RAW 264.7 macrophages (OB + MΦ). The cell seeded scaffolds produced with either small (112-224 μm) (A, C) or large (224-315 μm) (B, D) porogens were cultured in either control (ctrl) (white bars) or high calcium (high Ca) media (blue bars). From two scaffolds being cultured in the same bioreactor, one was loaded represented by the dashed bars, whereas the other was unloaded shown in blank white or blue bars.

a small amount of DNA detected on scaffolds with no cells seeded (figure 8.2 A, B). Comparing loaded and unloaded scaffolds in control media of both pore sizes, the DNA content was lower in loaded scaffolds besides in small pore scaffolds with just OB, whereas in high Ca media loaded scaffolds had more DNA than unloaded scaffolds (figure 8.2 A, B). The ALP activity on both pore size scaffolds was generally higher in scaffolds seeded with OB and MΦ especially in the high calcium media (figure 8.2 C, D). On scaffolds cultured in control media loaded ones had a lower ALP activity than unloaded scaffolds when cultured with OB, whereas loaded scaffolds had higher ALP activities when seeded with OB and MΦ. In the high calcium media just OB or OB in co-culture with MΦ had the same trend, the unloaded scaffolds had always a higher ALP activity (figure 8.2 C, D).

8.1.2 Mineralization over time monitored by microCT

All scaffolds seeded with or without cells cultured in control media showed no mineralization. The microCT data was used to visualize three-dimensional images of the mineralization on the scaffolds. As no big difference between loaded and unloaded scaffolds were observed microCT top view images of unloaded scaffolds cultured in high calcium media seeded with no cells, osteoblasts (OB) or osteoblasts and macrophages (OB + MΦ) on the two scaffold pore sizes were depicted in figure 8.3.

In both scaffolds the mineralization was increasing over time (figure 8.3). In small pore size scaffolds with no cells there was something detected at day 9 and 12, whereas more mineralization was detected on scaffolds with OB and even more and at an earlier time was detected on scaffolds seeded with OB and MΦ (figure 8.3). On large pore size scaffolds in all scaffolds with no cells, OB or OB and MΦ there was something detected starting at day 6 of culture and increasing in amount up to day 12 (figure 8.3).

Individual bone volume density values calculated from microCT data of day 2, 6, 9, and 12 of small and large pore size SF scaffolds seeded with no cells, just OB or OB and MΦ were presented in figure 8.4.

In both pore size scaffolds BV/TV values for scaffolds cultured in control media were detected at day 2, whereas they diminished at later culture time compared to scaffolds cultured in high calcium media (figure 8.4). Bone volume density in scaffolds cultured in high calcium media increased over time. In small pore size scaffolds bone volume density was increasing the most in scaffolds seeded with OB and MΦ up to around 0.9% (unloaded) or 0.7% (loaded), a bit less on scaffolds seeded with OB (day 12 BV/TV around 0.4% unloaded (ul) or 0.1 loaded (l)) and the detected BV/TV on scaffolds with no cells was increasing just a bit, not even up to 0.1% (unloaded and loaded) at day 12 (figure 8.4 A-D). On large pore size scaffolds cultured in high calcium media the bone volume density was measured to increase on all scaffolds in a similar way. The BV/TV values at day 12 were around 0.7% (ul) or 0.6% (l) for no cells, 0.5% (ul) and 0.75% (l) for just OB seeded and around 0.6% (ul) or 0.3% (l) for scaffolds seeded with OB and MΦ (figure 8.4 E-H). In both pore size scaffolds bone volume density was higher in unloaded scaffolds compared to loaded scaffolds, with just one exception in large pore size scaffolds where OB were seeded (figure 8.4.

To get a better visualization of the increase of bone volume density over time, the values of small and large pore size scaffolds cultured in high calcium media are plotted in a separate diagram, figure 8.5.

In figure 8.5 again the same findings can be made as already seen in figure 8.4.

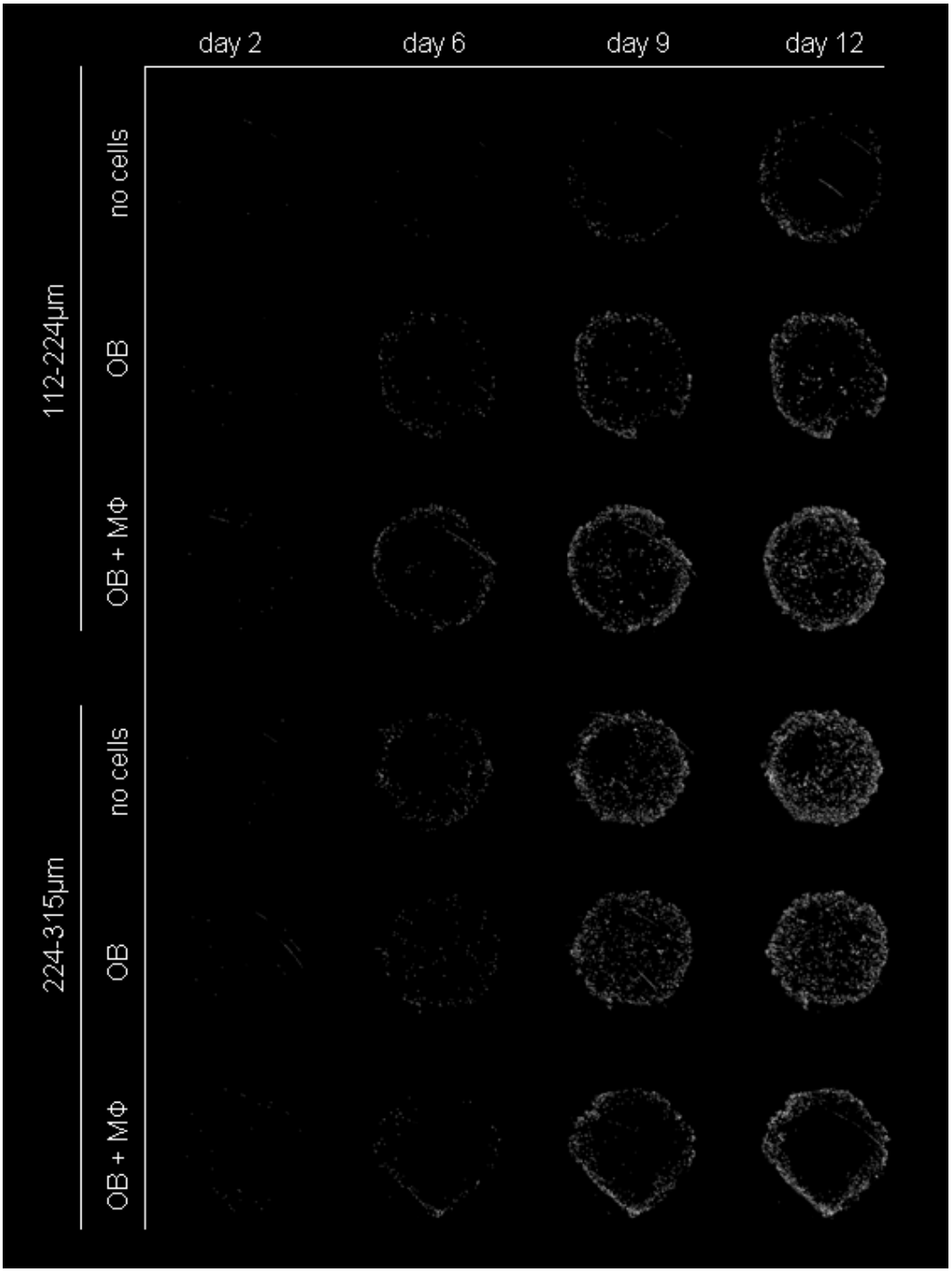

Figure 8.3: MicroCT top view images of no cells, OB or OB and Macrophages on small (112-224 μm porogens)or large pore size (224-315 μm porogens) SF scaffolds cultured in high Calcium medium for 13 days in bioreactors. The images show all unloaded scaffolds. Images are take at day 2, 6, 9 and 12 during culturing. The scaffold diameters are 5mm.

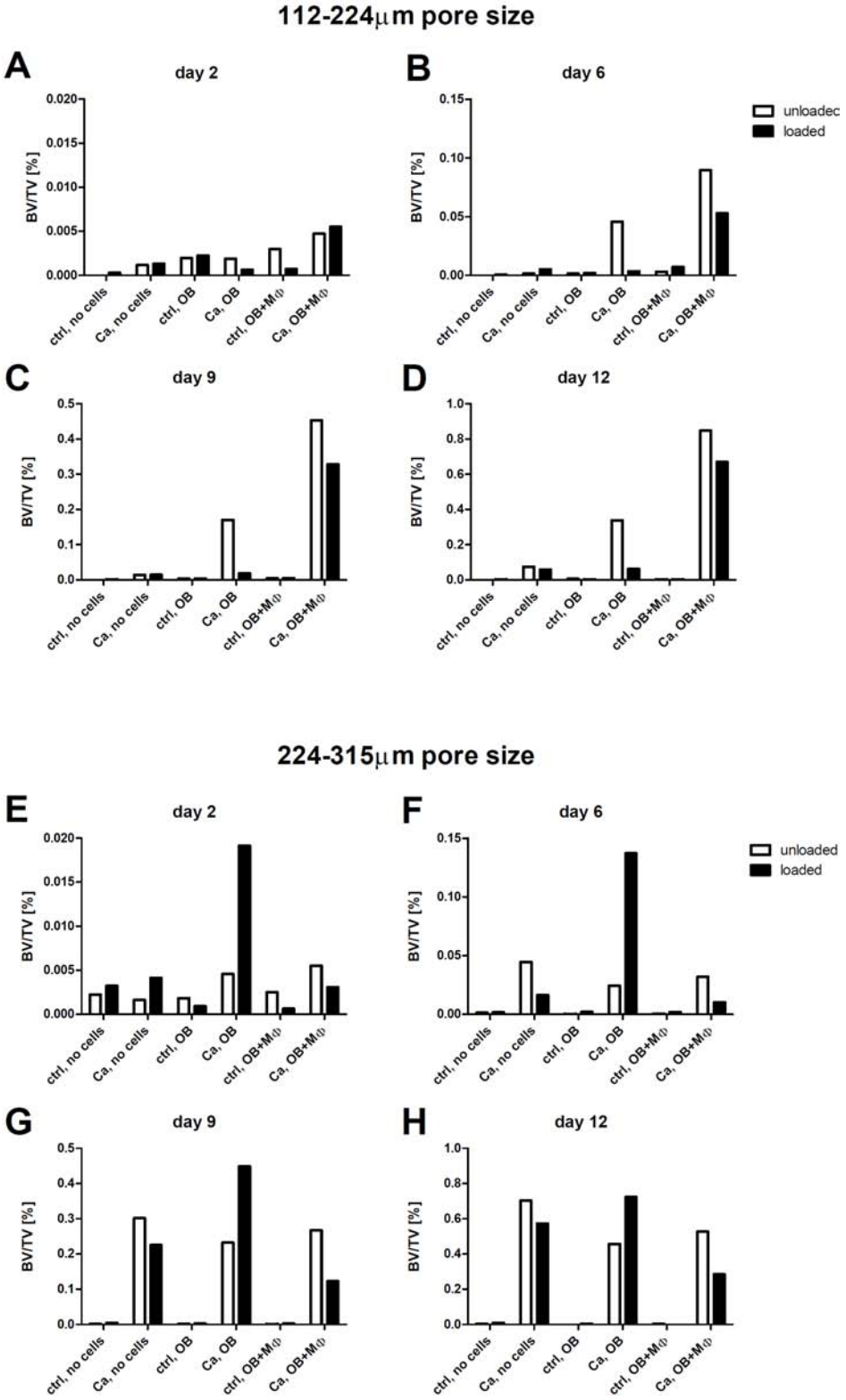

Figure 8.4: Bone volume density (BV/TV) of bone-like tissue constructs on small (A-D) or large (E-H) pore size SF scaffolds are shown from day 2, 6, 9 and 12 of culture. The cell seeded scaffolds were cultured in either control (ctrl) or high calcium (Ca) media with no cells, just OB or OB and MΦ seeded. The scaffolds were cultured in mechanical loading bioreactors. BV/TV of unloaded (white bars) and loaded (black bars) scaffolds are shown.

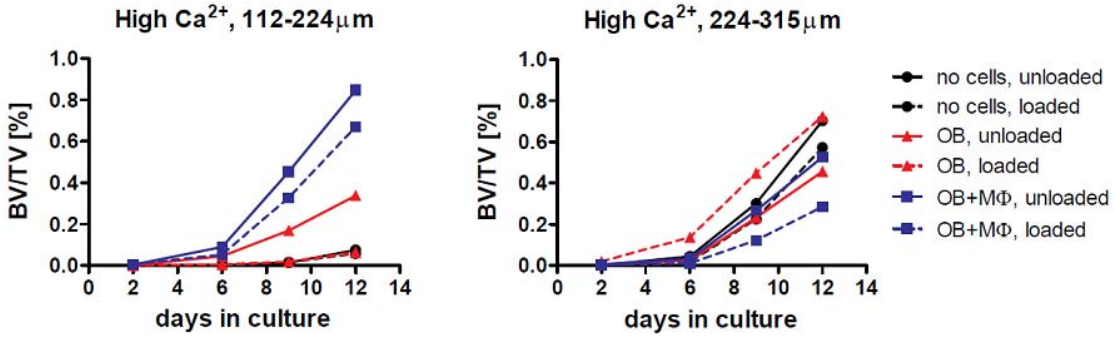

Figure 8.5: Bone volume density (BV/TV) increase during culture in high calcium media in scaffolds with two different pore sizes (112-224, 224-315 μm porogens) with either no cells (black lines), MC3T3 osteoblasts (OB) (red lines) or OB and RAW 264.7 macrophages (OB + MΦ) (blue lines). Values of unloaded scaffolds are shown as straight lines and of loaded scaffolds as dashed lines.

8.1.3 Histology and Immunohistochemistry

Histological sections were cut from all scaffold halves cultured for 13 days in control or high calcium media. Sections were stained with hematoxylin and eosin (H&E), Sirius Red, Alizarin Red S or von Kossa. In general is was very difficult to not destroy the sections during staining steps, as the sections probably were very fragile. Sections of a scaffold seeded with osteoblasts and stained for H&E, Sirius Red for collagen fibers, Alizarin Red for mineralization and von Kossa also for mineralization were shown in figure 8.6.

H&E stained sections was showing purple colored cell nuclei stained by hematoxylin and pink colored silk fibroin scaffold stained by eosin. There can be seen some cell nuclei within the silk fibroin scaffold structure (figure 8.6 A). Sirius Red was staining collagen fibers in red. In the section there are some fine structures stained positive for collagen (figure 8.6 B). Alizarin was staining calcium deposits and von Kossa phosphate deposits, so they are both stainings for mineralization. In figure 8.6 C and D there are some spots which are positively stained for mineralization.

To show, that seeded macrophages are still present on SF scaffolds after culture, immunohistochemical staining against macrophage marker F4/80 with a counter-staining with hematoxylin was done. Isotype control (rIgG2b) was performed at the same time to confirm specificity of staining. The IHC was based on a chromogen DAB, which colored identified antigens brown. To confirm the IHC staining, RAW 264.7 macrophages cultured on a glass slide were used as positive controls. Additionally C57BL/6 spleen sections were also used as positive controls to ensure proper dewaxing, rehydration and antigen retrieval on the sections. Images of F4/80 as well as matched isotype stain-

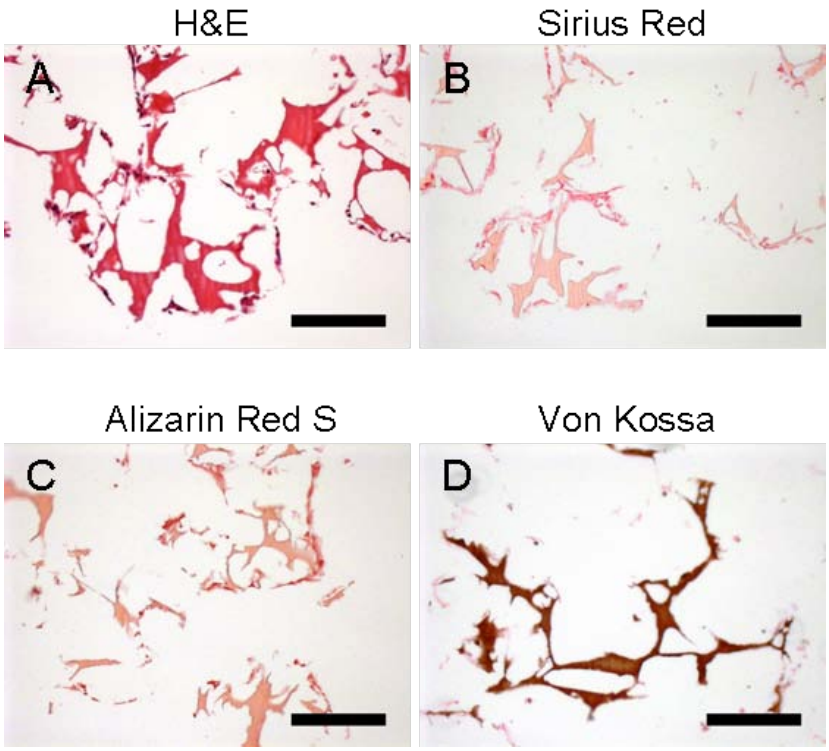

Figure 8.6: The images shows histological sections of 5 μm thickness of SF scaffold seeded with OB and cultured for 13 days in mechanical loading bioreactors. The sections were stained with Hematoxylin & Eosin, Sirius Red, Alizarin Red or von Kossa. The scale bars represent a length of 200 μm.

ings for RAW 264.7 cells, spleen sections and SF scaffold-cell construct sections seeded with MC3T3 osteoblasts and RAW 264.7 macrophages are depicted in figure 8.7. The arrows indicate a F4/80 positive cell and non-stained cells in the isotype control.

The IHC staining was shown to be positive for F4/80 positive RAW 264.7 macrophages (figure 8.7 A) with having background from unspecific binding (figure 8.7 B). The staining procedure was done on C57Bl/6 spleen sections, where a lot of macrophages are present in the red pulp (rp) but not in the white pulp (wp) of the spleen. Macrophages in the red pulp were positively stained for F4/80 (figure 8.7 C), although there was some unspecific background staining in the isotype stain observed (figure 8.7 D), as some cells were stained brown in the isotype control. Scaffold sections from SF scaffolds seeded with OB and MΦ showed, that macrophages were still present after culture within the SF scaffold (figure 8.7 E, G, I) and the isotype staining showed that also cells without any background staining were found (figure 8.7 F, H, J).

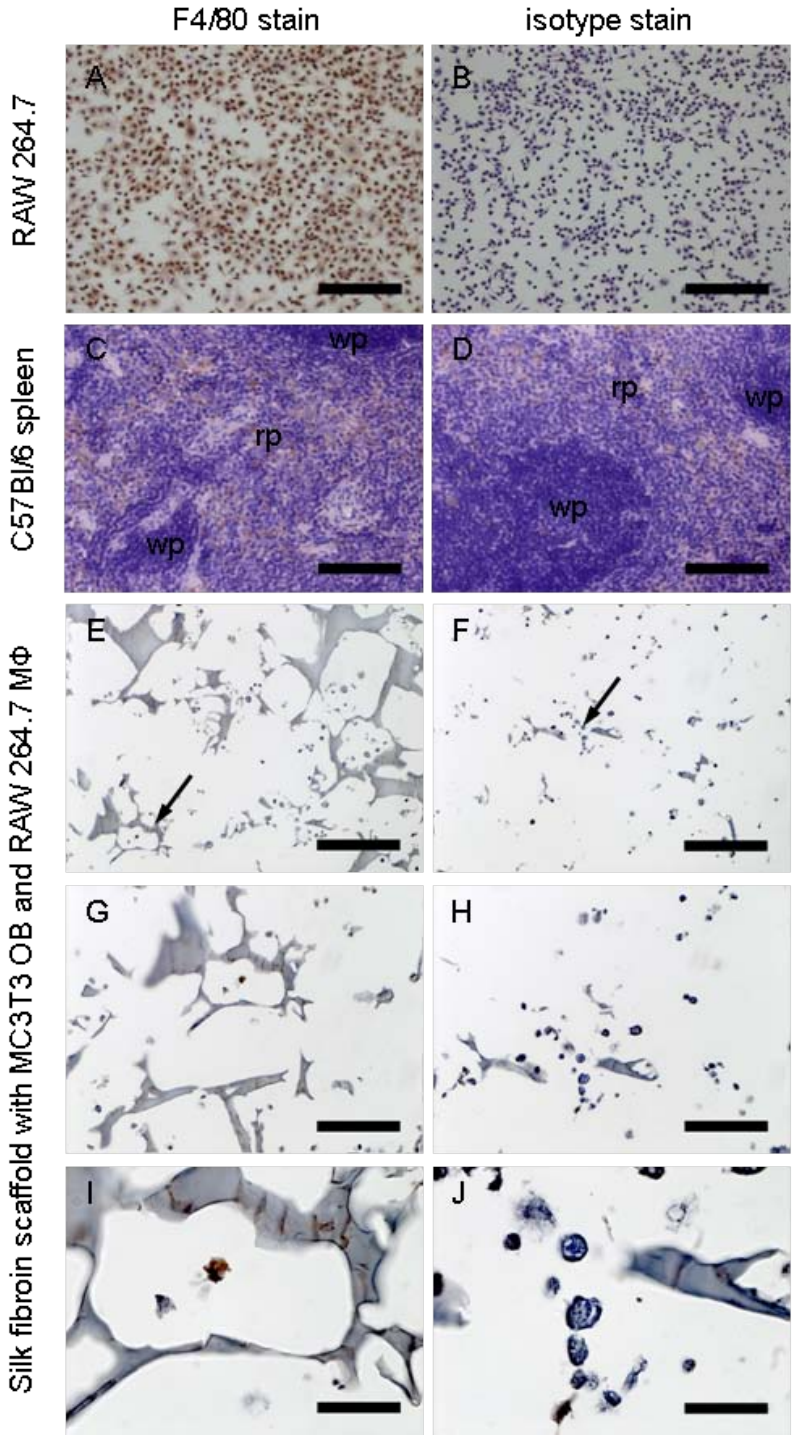

Figure 8.7: Immunohistochemical staining for F4/80$^+$ macrophages on serial sections of SF scaffolds cultured with MC3T3 osteoblasts and RAW 264.7 macrophages in mechanical loaded bioreactors (E-J). Staining for F4/80 (right column) and isotype-matched control staining with rIgG2b (left column) are shown. As control for the staining procedure RAW 264.7 macrophages cultured on a glass slide (A, B) and paraffin-embedded sections of C57BL/6 spleen (C,D) are depicted. Within the spleen white pulp (wp) and macrophage containing red pulp (rp) were observed. Scale bars represent 200 μm (A, B, E, F), 100 μm (C, D, G, H) or 50 μm (I, J).

8.2 Discussion

The biochemical assays (figure 8.2) showed, that DNA content was higher on scaffolds cultured in control media than scaffold cultured in high calcium media. This could be explained, as control media should not differentiate the cells into mature osteoblasts but rather stimulate them to proliferate, which was seen in a higher DNA content, as more cells were present. DNA assay compared to the ALP activity assay, which is a marker for osteoblast differentiation, showed, that cells which more proliferated had a lower ALP activity than cells which proliferated less. Indicating, that cells either start to proliferate or differentiate but not both together.

In the DNA assay (figure 8.2 A, B) there was measured also some DNA content on scaffolds with no cells. According to histological H&E sections there were no cells present on SF scaffolds without any cells seeded (data not shown), which would indicate that the measured DNA content could be taken as background of the DNA assay. It is known, that silk fibroin has autofluorescence [55] and therefore the background of the colorimetric DNA assay could be caused by autofluorescent silk fibroin dissolved in the measured samples. As for a DNA assay the SF scaffolds have to be destroyed, it is plausible, that small amounts of SF could be present in the actual samples where DNA content was measured on.

ALP activity was higher in scaffolds with OB and MΦ in co-culture than with just OB seeded. Taking into account, that the readings were normalized against DNA content, including DNA of macrophages, which should not express ALP, the ALP activity per OB would probably give even higher values for scaffolds with OB + MΦ seeded. Therefore, the trend looks like that high calcium media in combination with macrophages in co-culture showed osteogenic characteristics for osteoblasts, meaning that osteoblastic progenitor cells were stimulated to differentiate into osteoblasts. Especially unloaded co-cultures of osteoblast precursor cells with macrophages were seen to result in the highest ALP activities, meaning the most OB differentiation, which is in accordance with the experiments by Chang *et al.* [10, 38].

MicroCT monitoring of the mineralization during culture showed, that in scaffolds cultured in control media no mineralization occured. This is in accordance to DNA and ALP activity assays, as the cells on this scaffolds were also not much differentiated but rather proliferated. In all scaffold cultured in high calcium media, there was some increasing mineralization detected. On scaffolds with no cells seeded this detected signal could hardly be from real mineralization, as in histological sections no cells were confirmed. A good explanation would be, that calcium from the high calcium media precipitated on the SF scaffolds. As in high calcium media a concentration of

4mM $CaCl_2$ was used, which is around 4 times higher than calcium concentrations used in standard osteogenic medias, a precipitation is very plausible. In scaffolds with small pore sizes this precipitation was relatively low and up to 9 times less than mineralization observed in scaffolds with cells. Large pore size scaffolds although had precipitations in scaffolds with no cells, which reached the levels of scaffolds seeded with cells. With the microCT technique one could not distinguish if this precipitation and the mineralization found on cell-hosted scaffolds had the same chemical structure or not. To identify differences one would need a structural analysis, as e.g. energy-dispersive X-ray spectroscopy (EDX) or Raman spectroscopy, which could detect if the mineralization was hydroxyapatite-like, as in natural bone or if the precipitation was just pure calcium [17]. Still, there is the question why in large pore size scaffolds the calcium precipitated much more then in small pore size scaffolds. It may be that the large pore size scaffolds were more prone to precipitations than small pore size scaffolds due to their scaffold architecture. Morphometric indices measured with microCT on the two scaffold types showed, that large pore size scaffolds had less scaffold surface and higher wall thickness compared to small pore size scaffolds. Thus, a higher precipitation could be explained, if the calcium infiltrates the scaffold structure and due to thicker wall more calcium could accumulate in large pore size scaffolds. There might be also a difference in pore connectivity as in large pore size scaffolds the precipitation reached faster the inside of the scaffolds.

Mechanical loading of the cells did not stimulate the cells to differentiate but to proliferate, according to higher DNA content and lower ALP activities compared to unloaded scaffolds. This then is in contrast to the hypothesis that loading increases differentiation and therefore osteoblast mineralization of SF scaffolds. Also the microCT data showed, that loading did not help to increase mineralization rate, mechanically loaded scaffolds had even less mineralization than unloaded scaffolds. Although, this setup with two scaffolds per bioreactor does not allow to investigate the effect of soluble factors produced by the stimulated cells in the loaded scaffolds, as the cells on the unloaded scaffold also would be influenced by any soluble factors. Therefore, any trends seen by mechanical stimulation could be just explained with cell-cell interactions and not with soluble factors. It seemed, that loading even decreased mineralization rates. Therefore the question whether loading per se would not help arises. Another possibility was that the loading parameters were not optimal, although Reilly *et al.* showed, that with the same loading parameters helped to increase mineralization of an other osteoblast cell line on polyurethane scaffolds [44]. The loading was cyclic as it was proposed by Duncan *et al.* [15] to have an effect. It might be that the strains acting on the cells were too high, which would according to Jones *et al.* [27]

de-differentiate the cells rather than stimulate further differentiation. Or it could be, that stimulation was too early, as cells just attached to the scaffolds and which may be rather disturbing for the cells than stimulating to differentiate. An experiment, where cells seeded on SF scaffolds first are cultured for a certain time until there is already clear mineralization observed and then mechanical stimulation would be applied, to see if mechanical loading would help in a later stage of the mineralization process would be worth investigating. To eliminate the interactions of possible soluble factors from mechanical stimulation on unloaded cells, the unloaded and loaded scaffolds should be separated in any further experiments.

H&E sections (figure 8.6) of all scaffolds cultured in MSU bioreactors showed the presence of cells in the SF scaffold seeded with cells. Evaluating scaffold sections was rather difficult, as most of the scaffolds got destroyed during staining processes. This may be due to relatively low stability of the sections as they were not yet mineralized so being probably rather fragile and the scaffolds were porous, which had as consequence less scaffold area which could attach to the glass slide.

The IHC staining of scaffold sections where OB and MΦ were seeded on showed, that in the scaffolds after culture macrophages were still present. The IHC staining needs to be further optimized, as in murine spleen sections there was unwanted background staining detected. The activation of macrophages due to the silk fibroin was not investigated in this study, as previously was shown, that purified silk fibroin does not induce any macrophage reactions [34].

Generally, on small pore size scaffolds mineralization rate was increased if osteoblasts were co-cultured with macrophages in high calcium media, which simulates an physiologic anabolic stimuli. Although mechanical loading did not increase mineralization rate. Comparing the results with the initial hypothesis, the results reject the hypothesis as mechanical loading was even lowering mineralization rate. But still, macrophages have been shown at least in small pore size SF scaffolds, to enhance osteoblast differentiation and therefore increased mineralization rate in response to elevated extracellular calcium.

Chapter 9

Conclusion and Outlook

Silk fibroin scaffolds with two different pore sizes were produced and characterized. Different SF batches resulted in non structurally different SF scaffolds.

MC3T3 osteoblast cell line was cultured successfully in 2D. It has been found, that BGJb media with osteogenic factors promoted cell differentiation into osteoblasts best and physiologically similar mineralization nodules as well as collagen distribution within the cell layer indicated bone-like tissue formation. Different cell seeding densities revealed no significant differences showing, that the lowest cell seeding density of 1.2 x 10^4 cells/well was sufficient.

MC3T3 were successfully cultured in 3D on SF scaffolds in osteogenic BGJb media in static bioreactors for 33 days. Biochemical assays and histological analysis showed, that MC3T3 were differentiating into osteoblasts and produced collagen and started to mineralize the ECM. Overall, MC3T3 osteoblasts were shown to produce bone-like tissue if cultured on SF scaffolds of either smaller or larger pore sizes.

As a competitive tissue-engineered bone graft should be provided in a short time, the osteoblast differentation and mineralization rate was tried to be increased with using two different stimuli. On one hand mechanical stimulation to MC3T3 osteoblasts cultured on SF scaffolds was applied by a cyclic load-induced stimulation of the scaffold. On the other hand osteoblast differentiation was stimulated using a co-culture of RAW 264.7 macrophages in high calcium media simulating elevated extracellular calcium. MC3T3 and RAW 264.7 macrophages were cultured on both scaffold types in mechanical loading bioreactors, loaded 5 times during culturing. The hypothesis, that both stimuli togother enhance osteoblast mineralization needs to be rejected, as mechanical loading with the used parameters rather hindered mineralization on SF scaffolds.

Taken together, SF scaffolds were shown to promote bone-like tissue formation of MC3T3 osteoblasts in 3D and as shown before where biocompatible and biodegradable

in vivo. Co-culturing macrophages with osteoblasts was shown to enhance bone-like tissue formation of MC3T3 on SF scaffolds.

As an outlook, it would be worth to find methods, which allow production of more homogenous SF scaffolds, which then should reduce effects of scaffold diversity in the cell culture and facilitate interpretation of results.

In future experiments, percipitation observed in control scaffolds should be analyzed structurally and compared to mineralization found on cell seeded scaffolds. An experiment, which investigates if already a lower calcium concentration in the media would be sufficient to enhance osteoblast differentiation in co-culture with macrophages should be conducted. As a lower calcium concentration in the media would reduce the possibility of spontaneous calcium precipitation on the scaffolds to allow investigations on cell produced mineralization.

The results of an experiment with MC3T3 cocultured with macrophages in perfusion bioreactors or also spinner flask bioreactors would be very interesting. As a perfusion of the scaffolds would enhance nutrient and metabolite exchange within the scaffolds, osteoblasts should be able to survive in the whole scaffold. This would be needed to engineer uniformly mineralized bone tissue grafts. The loading of osteoblasts on SF scaffold had no enhancing effect, although it should be investigated if other loading parameters or loading at a later time in culture, when already some mineralization is present, could increase osteoblast mineralization rate.

The effect of macrophages on osteoblast differentation and bone tissue formation using an osteoblast cell line MC3T3 was important to investigate, though to get more clinically relevance an osteoblast/macrophage co-culture should also investigated with human derived cells, such as human mesenchymal stem cells able to differentiate into osteoblasts and human derived macrophages.

As a longterm aim, upscaling of scaffolds with optimized mineralization rate should be conducted to once be able to provide tissue-engineered bone grafts matching needed graft dimensions. One of the major problems need to be solved if scaffolds are upscaled is, that from a ceratin scaffold size nutrient and metabolie transport and exchange will be a restricting problem. This could be solved by vascularization of the tissue-engineered bone.

Overall, bone tissue formation was shown to be enhanced by co-culturing osteoblasts toghether with macrophages. As for a bone graft the bone tissue would be needed in a short time, macrophage enhanced bone formation could be an additional component allowing to bring tissue engineering once into clinical relevant applications.

Bibliography

[1] Altman, G. H., Diaz, F., Jakuba, C., Calabro, T., Horan, R. L., Chen, J. S., Lu, H., Richmond, J., and Kaplan, D. L. Silk-based biomaterials. *Biomaterials 24*, 3 (2003), 401–416.

[2] Andersen, L., Contera, S., Justesen, J., Duch, M., Hansen, O., Chevallier, J., Foss, M., Pedersen, F., and Besenbacher, F. Cell volume increase in murine mc3t3-e1 pre-osteoblasts attaching onto biocompatible tantalum observed by magnetic ac mode atomic force microscopy. *Eur Cell Mater 10* (2005), 61–8; discussion 68–9.

[3] Arron, J. R., and Choi, Y. Osteoimmunology - bone versus immune system. *Nature 408*, 6812 (2000), 535–536.

[4] Bartel, D. L., D., D. T., and M., K. T. The musculoskeletal system. In *Orthopaedic biomechanics: mechanics and design in musculoskeletal systems*. Pearson Education, Inc., Upper Saddle River, New Jersey, 2006, pp. 1–22.

[5] Biewener, A. A., Fazzalari, N. L., Konieczynski, D. D., and Baudinette, R. V. Adaptive changes in trabecular architecture in relation to functional strain patterns and disuse. *Bone 19*, 1 (1996), 1–8.

[6] Bonewald, L. F. Osteocytes. In *Primer on the Metabolic Bone Diseases and Disorders of Mineral Metabolism*, C. J. Rosen, Ed., 7th ed. American Society for Bone and Mineral Research, Washington, DC, 2008, pp. 22–27.

[7] Bueno, E. M., Bilgen, B., Carrier, R. L., and Barabino, G. A. Increased rate of chondrocyte aggregation in a wavy-walled bioreactor. *Biotechnology and Bioengineering 88*, 6 (2004), 767–777.

[8] Caetano-Lopes, J., Canhao, H., and Fonseca, J. E. Osteoimmunology - the hidden immune regulation of bone. *Autoimmunity Reviews 8*, 3 (2009), 250–255.

[9] Cao, Y., and Wang, B. C. Biodegradation of silk biomaterials. *International Journal of Molecular Sciences 10*, 4 (2009), 1514–1524.

[10] Chang, M. K., Raggatt, L. J., Alexander, K. A., Kuliwaba, J. S., Fazzalari, N. L., Schroder, K., Maylin, E. R., Ripoll, V. M., Hume, D. A., and Pettit, A. R. Osteal tissue macrophages are intercalated throughout human and mouse bone lining tissues and regulate osteoblast function in vitro and in vivo. *Journal of Immunology 181*, 2 (2008), 1232–1244.

[11] Chang, Y., Stanford, C., and Keller, J. Calcium and phosphate supplementation promotes bone cell mineralization: implications for hydroxyapatite (ha)-enhanced bone formation. *J Biomed Mater Res 52*, 2 (2000), 270–8.

[12] Chen, H. C., and Hu, Y. C. Bioreactors for tissue engineering. *Biotechnology Letters 28*, 18 (2006), 1415–1423.

[13] Chou, Y. F., Dunn, J. C. Y., and Wu, B. M. In vitro response of mc3t3-e1 preosteoblasts within three-dimensional apatite-coated plga scaffolds. *Journal of Biomedical Materials Research Part B-Applied Biomaterials 75B*, 1 (2005), 81–90.

[14] Duncan, R. L., and Hruska, K. A. Chronic, intermittent loading alters mechanosensitive channel characteristics in osteoblast-like cells. *American Journal of Physiology-Renal Physiology 267*, 6 (1994), F909–F916.

[15] Duncan, R. L., and Turner, C. H. Mechanotransduction and the functional-response of bone to mechanical strain. *Calcified Tissue International 57*, 5 (1995), 344–358.

[16] Freyria, A. M., Yang, Y., Chajra, H., Rousseau, C. F., Ronziere, M. C., Herbage, D., and El Haj, A. J. Optimization of dynamic culture conditions: Effects on biosynthetic activities of chondrocytes grown in collagen sponges. *Tissue Engineering 11*, 5-6 (2005), 674–684.

[17] Gentleman, E., Swain, R., Evans, N., Boonrungsiman, S., Jell, G., Ball, M., Shean, T., Oyen, M., Porter, A., and Stevens, M. Comparative materials differences revealed in engineered bone as a function of cell-specific differentiation. *Nat Mater 8*, 9 (2009), 763–70.

[18] Giannoudis, P., Dinopoulos, H., and Tsiridis, E. Bone substitutes: an update. *Injury 36 Suppl 3* (2005), S20–7.

[19] Goldring, S., and Goldring, M. Eating bone or adding it: the wnt pathway decides. *Nat Med 13*, 2 (2007), 133–4.

[20] Gosline, J. M., Guerette, P. A., Ortlepp, C. S., and Savage, K. N. The mechanical design of spider silks: From fibroin sequence to mechanical function. *Journal of Experimental Biology 202*, 23 (1999), 3295–3303.

[21] Hagenmüller, H. *Combining micro-computed tomography monitoring and mechanical loading in bone tissue engineering.* PhD thesis, 2009.

[22] Hagenmüller, H., Hitz, M., Merkle, H., Meinel, L., and Müller, R. Design and validation of a novel bioreactor principle to combine online micro-computed tomography monitoring and mechanical loading in bone tissue engineering. *Rev Sci Instrum 81*, 1 (2010), 014303.

[23] Heersche, J. N. M. Mechanism of osteoclastic bone-resorption - new hypothesis. *Calcified Tissue Research 26*, 1 (1978), 81–84.

[24] Hofmann, S., Hagenmuller, H., Koch, A. M., Muller, R., Vunjak-Novakovic, G., Kaplan, D. L., Merkle, H. P., and Meinel, L. Control of in vitro tissue-engineered bone-like structures using human mesenchymal stem cells and porous silk scaffolds. *Biomaterials 28*, 6 (2007), 1152–1162.

[25] Jaasma, M. J., and O'Brien, F. J. Mechanical stimulation of osteoblasts using steady and dynamic fluid flow. In *2nd Annual Meeting of the European Chapter of the Tissue-Engineering-and-Regenerative-Medicine-International-Society* (2007), vol. 14, pp. 1213–1223.

[26] Jaiswal, N., Haynesworth, S. E., Caplan, A. I., and Bruder, S. P. Osteogenic differentiation of purified, culture-expanded human mesenchymal stem cells in vitro. *Journal of Cellular Biochemistry 64*, 2 (1997), 295–312.

[27] Jones, D. B., Nolte, H., Scholubbers, J. G., Turner, E., and Veltel, D. Biochemical signal transduction of mechanical strain in osteoblast-like cells. In *1990 Conf on Biointeractions (Biointeractions 90)* (1990), vol. 12, pp. 101–110. 2.

[28] Kim, U. J., Park, J., Kim, H. J., Wada, M., and Kaplan, D. L. Three-dimensional aqueous-derived biomaterial scaffolds from silk fibroin. *Biomaterials 26*, 15 (2005), 2775–2785.

[29] Krause, C. J., de Gorter D. J. J., Karperien, M., and ten Dijke P. Signal transduction cascades controlling osteoblast differentiation. In *Primer on the Metabolic Bone Diseases and Disorders of Mineral Metabolism*, C. J. Rosen, Ed., 7th ed. American Society for Bone and Mineral Research, Washington, DC, 2008, pp. 10–16.

[30] Meinel, L., Hofmann, S., Karageorgiou, V., Kirker-Head, C., McCool, J., Gronowicz, G., Zichner, L., Langer, R., Vunjak-Novakovic, G., and Kaplan, D. L. The inflammatory responses to silk films in vitro and in vivo. *Biomaterials 26*, 2 (2005), 147–155.

[31] Nazarov, R., Jin, H. J., and Kaplan, D. L. Porous 3-d scaffolds from regenerated silk fibroin. *Biomacromolecules 5*, 3 (2004), 718–726.

[32] Ozawa, H., Imamura, K., Abe, E., Takahashi, N., Hiraide, T., Shibasaki, Y., Fukuhara, T., and Suda, T. Effect of a continuously applied compressive pressure on mouse osteoblast-like cells (mc3t3-e1) invitro. *Journal of Cellular Physiology 142*, 1 (1990), 177–185.

[33] Palomares, K. T. S., Gleason, R. E., Mason, Z. D., Cullinane, D. M., Einhorn, T. A., Gerstenfeld, L. C., and Morgan, E. F. Mechanical stimulation alters tissue differentiation and molecular expression during bone healing. *Journal of Orthopaedic Research 27*, 9 (2009), 1123–1132.

[34] Panilaitis, B., Altman, G., Chen, J., Jin, H., Karageorgiou, V., and Kaplan, D. Macrophage responses to silk. *Biomaterials 24*, 18 (2003), 3079–85.

[35] Perez-Rigueiro, J., Viney, C., Llorca, J., and Elices, M. Mechanical properties of single-brin silkworm silk. *Journal of applied polymer science 75*, 10 (2000), 1270–1277.

[36] Pettit, A. R., Chang, M. K., Hume, D. A., and Raggatt, L. J. Osteal macrophages: A new twist on coupling during bone dynamics. *Bone 43*, 6 (2008), 976–982.

[37] Quarles, L. D., Yohay, D. A., Lever, L. W., Caton, R., and Wenstrup, R. J. Distinct proliferative and differentiated stages of murine mc3t3-e1 cells in culture - an invitro model of osteoblast development. *Journal of Bone and Mineral Research 7*, 6 (1992), 683–692.

[38] Raggatt, L. J., Chang, M. K., Alexander, K. A., Maylin, E. R., Walsh, N. C., Gravallese, E. M., Hume, D. A., and Pettit, A. R. Osteomacs: Osteoclast precursors during inflammatory bone disease but regulators of physiologic bone remodeling. In *2nd Joint Meeting of the International-Bone-and-Mineral-Society/Australian-New-Zealand-Bone-and-Mineral-Society* (2009), vol. 44, p. 386.

[39] Ralph, P., and Nakoinz, I. Antibody-dependent killing of erythrocyte and tumor targets by macrophage-related cell lines - enhancement by ppd and lps. *Journal of Immunology 119*, 3 (1977), 950–954.

[40] Raschke, W. C., Baird, S., Ralph, P., and Nakoinz, I. Functional macrophage cell lines transformed by abelson leukemia-virus. *Cell 15*, 1 (1978), 261–267.

[41] Robey, P. G., and Boskey, A. L. The composition of bone. In *Primer on the Metabolic Bone Diseases and Disorders of Mineral Metabolism*, C. J. Rosen, Ed., 7th ed. American Society for Bone and Mineral Research, Washington, DC, 2008, pp. 32–38.

[42] Ross, F. P. Osteoclast biology and bone resorption. In *Primer on the Metabolic Bone Diseases and Disorders of Mineral Metabolism*, C. J. Rosen, Ed., 7th ed. American Society for Bone and Mineral Research, Washington, DC, 2008, pp. 16–22.

[43] Sabir, M. I., Xu, X. X., and Li, L. A review on biodegradable polymeric materials for bone tissue engineering applications. *Journal of Materials Science 44*, 21 (2009), 5713–5724.

[44] Sittichockechaiwut, A., Scutt, A., Ryan, A., Bonewald, L., and Reilly, G. Use of rapidly mineralising osteoblasts and short periods of mechanical loading to accelerate matrix maturation in 3d scaffolds. *Bone 44*, 5 (2009), 822–9.

[45] Stauber, M., and Müller, R. Micro-computed tomography: a method for the non-destructive evaluation of the three-dimensional structure of biological specimens. *Methods Mol Biol 455* (2008), 273–92.

[46] Stock, U. A., and Vacanti, J. P. Tissue engineering: Current state and prospects. *Annual Review of Medicine 52* (2001), 443–451.

[47] Sudo, H., Kodama, H., Amagai, Y., Yamamoto, S., and Kasai, S. In vitro differentiation and calcification in a new clonal osteogenic cell line derived from newborn mouse calvaria. *J Cell Biol 96*, 1 (1983), 191–8.

[48] Takayanagi, H., Ogasawara, K., Hida, S., Chiba, T., Murata, S., Sato, K., Takaoka, A., Yokochi, T., Oda, H., Tanaka, K., Nakamura, K., and Taniguchi, T. T-cell-mediated regulation of osteoclastogenesis by signalling cross-talk between rankl and ifn-gamma. *Nature 408*, 6812 (2000), 600–605.

[49] Uebersax, L., Hagenmueller, H., Hofmann, S., Gruenblatt, E., Mueller, R., Vunjak-Novakovic, G., Kaplan, D. L., Merkle, H. P., and Meinel, L. Effect of scaffold design on bone morphology in vitro. In *Workshop on Tissue Engineering - The Next Generation* (Boston, MA, 2005), vol. 12, pp. 3417–3429.

[50] Wang, D., Christensen, K., Chawla, K., Xiao, G., Krebsbach, P., and Franceschi, R. Isolation and characterization of mc3t3-e1 preosteoblast subclones with distinct in vitro and in vivo differentiation/mineralization potential. *J Bone Miner Res 14*, 6 (1999), 893–903.

[51] Wang, Y., Rudym, D. D., Walsh, A., Abrahamsen, L., Kim, H. J., Kim, H. S., Kirker-Head, C., and Kaplan, D. L. In vivo degradation of three-dimensional silk fibroin scaffolds. *Biomaterials 29*, 24-25 (2008), 3415–3428.

[52] Wen, C., Ye, S., Zhou, L., and Yu, Y. Silk-induced asthma in children - a report of 64 cases. *Annals of Allergy 65*, 5 (1990), 375–378.

[53] Wong, B. R., Josien, R., and Choi, Y. Trance is a tnf family member that regulates dendritic cell and osteoclast function. *Journal of Leukocyte Biology 65*, 6 (1999), 715–724.

[54] Wüest, S. Optimization of extracellular matrix production on silk scaffolds. Master's thesis, ETH Zurich, Institute for Biomechanics, 2009.

[55] Yang, Y., Shao, Z., Chen, X., and Zhou, P. Optical spectroscopy to investigate the structure of regenerated bombyx mori silk fibroin in solution. *Biomacromolecules 5*, 3 (2004), 773–9.

Statement regarding plagiarism when submitting written work at ETH Zurich

By signing this statement, I affirm that I have read the information notice on plagiarism, independently produced this paper, and adhered to the general practice of source citation in this subject-area.

Beiblatt zu an der ETH Zürich verfassten schriftlichen Arbeiten

Ich erkläre mit meiner Unterschrift, das Merkblatt Plagiat zur Kenntnis genommen, die vorliegende Arbeit selbständig verfasst und die im betroffenen Fachgebiet üblichen Zitiervorschriften eingehalten zu haben.

Information notice on plagiarism: http://www.ethz.ch/students/semester/plagiarism_s_en.pdf
Merkblatt Plagiat: http://www.ethz.ch/students/semester/plagiarism_s_de.pdf

_____ _____

Place and date signature / Ort, Datum Unterschrift